Supplemental Information

Reaction kinetics and multi-sulfur products formation of sulfur-containing volatile organic compounds with OH radicals

Xun Rong[1], Lei Yao[1,2,3]*, Chuang Li[1], Cong An[1], Gan Yang[1], Jiali Shen[3], Runlong Cai[1,2], Douglas R. Worsnop[3,4], Lin Wang[1,2,3,6,7]

[1] Shanghai Key Laboratory of Air Quality and Environmental Health, Department of Environmental Science and Engineering, Jiangwan Campus, Fudan University, Shanghai 200438, China

[2] Shanghai Institute of Pollution Control and Ecological Security, Shanghai 200092, China

[3] National Observations and Research Station for Wetland Ecosystems of the Yangtze Estuary, Shanghai 200438, China

[4] Institute for Atmospheric and Earth System Research/Physics, Faculty of Science, University of Helsinki, 00014 Helsinki, Finland

[5] Aerodyne Research, Billerica, MA 01821, USA

[6] IRDR International Center of Excellence on Risk Interconnectivity and Governance on Weather/Climate Extremes Impact and Public Health, Fudan University, Shanghai 200438, China

[7] Collaborative Innovation Center of Climate Change, Nanjing, 210023, China

**Corresponding Author: L.Y., email, lei_yao@fudan.edu.cn*

Text S1. Vocus-PTR-LToF-MS and nitrate-CI-LToF-MS.

The Vocus-PTR-LToF-MS was employed to monitor the evolution of sulfur-VOCs in our chamber during the oxidation process with the time resolution of 1 Hz. This instrument operates through proton transfer reactions between H_3O^+ ions and target VOCs with proton affinity greater than that of water. The mass resolution of Vocus-PTR-LToF-MS was ~12,000 at *m/z* 200 Th. The instrument was calibrated with sulfur-VOC standards and background signals were determined by introducing zero air.

The nitrate-CI-LToF-MS was used to measure and identify the oxidation products formed from the reactions of sulfur-VOCs with •OH. This instrument employs $(HNO_3)_n \cdot NO_3^-$ cluster to selectively ionize oxidized molecules, demonstrating a resolving power up to 8000 for ions with *m/z*>200 Th. Mass calibration was performed using NO_3^-, $HNO_3 \cdot NO_3$-, and $(HNO_3)_2 \cdot NO_3^-$ ions. For identification of sulfur-containing oxygenated organic molecules (sulfur-OOMs), mass accuracy was maintained below 4 ppm.

Text S2. •OH generation and kinetic constants of sulfur-VOCs and •OH.

•OH were generated by the photolysis of O_3/H_2O mixtures using a UV lamp,

$$O_3 + hv\ (253nm) \rightarrow O_2 + O(^1D) \qquad \text{R. (1)}$$

$$O(^1D) + H_2O \rightarrow 2\bullet OH \qquad \text{R. (2)}$$

The experimental conditions maintained an O_3 concentration of approximately 31 ppbv and a RH of 24%, suggesting comparable •OH concentrations across all chamber simulation experiments of sulfur-VOCs with stable •OH levels throughout the reactions. Based on the temperature-dependent rate constant for the DMS-•OH reaction from IUPAC recommendations ($k_{DMS} = 8.1\times10^{-12}$ cm^3 $molecule^{-1}$ s^{-1} at 291 K and 1 atm), and correlating with the linear fitting results of DMS and •OH reaction experiments, the •OH concentration in the reaction chamber was estimated to be approximately $(4.42 \pm 0.08) \times10^7$ molecules cm^{-3}.

Considering the wall loss and dilution loss of sulfur-VOCs in the reaction chamber, the reaction rate constant was calculated using Eq. (1):

$$\left[\ln\frac{[\text{sulfur-VOC}]_t}{[\text{sulfur-VOC}]_0}\right]_\alpha - \left[\ln\frac{[\text{sulfur-VOC}]_t}{[\text{sulfur-VOC}]_0}\right]_\beta = -k_{\text{sulfur-VOC}}\cdot[\bullet OH]\cdot t \qquad \text{Eq. (1)}$$

where the term with the subscript α represents the change in sulfur-VOC concentration over time t when the UV lamp is turned on, comprising three consuming pathways: reaction with •OH, wall loss, and dilution loss; the term with the subscript β represents the change when the UV lamp is turned off, comprising only wall loss and dilution loss. The difference between the two reflects the change in the reaction between sulfur-VOC and •OH, which follows first-order reaction kinetics. The slope obtained from linear fitting is the product of $k_{\text{sulfur-VOC}}$ and [•OH].

Text S3. Wall and dilution loss of sulfur-VOCs in our chamber experiments

As shown in Figure S5, the temporal concentration profiles of 5 sulfur-VOCs including ethanethiol

(C_2H_6S), 1-propanethiol (C_3H_8S), dimethyl sulfide (C_2H_6S), methyl ethyl sulfide (C_3H_8S) and bis(methylthio)methane ($C_3H_8S_2$), were characterized by linear fitting to quantify their wall loss and dilution loss rates. However, for other 6 sulfur-VOCs (i.e., 2-propanethiol (C_3H_8S), 1,2-ethanedithiol ($C_2H_6S_2$), 1,3-propanedithiol ($C_3H_8S_2$), trimethylene sulfide (C_3H_6S), 1,3-dithiolane ($C_3H_6S_2$) and dimethyl disulfide ($C_2H_6S_2$)) that were rapidly consumed during the •OH oxidation phase, no measurable concentration decay attributable solely to wall loss or dilution loss could be obtained after the UV lamps were turned off. Consequently, the wall loss and dilution loss derived from DMS were applied as proxies for these 6 sulfur-VOCs.

Text S4. Calibration of Vocus-PTR-LToF-MS using standard sulfur-VOCs

A mixture of calibration gases containing methanethiol, DMS, ethyl methyl sulfide, and DMDS was used to calibrate the Vocus-PTR-LToF-MS for quantifying sulfur-VOCs selected in our chamber experiments and emitted from freshwater algae samples. The original mixing ratios of these four reduced sulfur compounds in the standard mixture were 1.0 ppmv (parts per million by volume) (Weichuang Gas Ltd., China). To ensure that the calibration is applicable to atmospherically relevant levels of sulfur-VOCs, the standard mixture was diluted with high-purity N_2 to the pptv levels. As shown in Figure S14, the resulting sensitivities for methanethiol, DMS, ethyl methyl sulfide, and DMDS were 0.61, 0.92, 0.57, and 0.82 cps $pptv^{-1}$, respectively. For freshwater algae emitted sulfur-VOCs without compound-specific calibrations, the sensitivity of DMS was applied to quantify mono-sulfur organic species, whereas the sensitivity of DMDS was adopted to quantify multi-sulfur organic species.

Text S5. Semi-quantification of multi-sulfur products

Multi-sulfur product concentrations are quantified by Eq. (2)

$$[\text{multi-sulfur product}] = C \times \frac{(\text{multi-sulfur product})^- + (\text{multi-sulfur product})\cdot NO_3^-}{NO_3^- + HNO_3NO_3^- + (HNO_3)_2NO_3^-} \quad \text{Eq. (2)}$$

Where $(\text{multi-sulfur product})^-$, $(\text{multi-sulfur product})\cdot NO_3^-$, NO_3^-, $HNO_3NO_3^-$, and $(HNO_3)_2NO_3^-$ represent signals of corresponding ions in units of counts per second (cps). For quantification, we assume that multi-sulfur products containing two or more oxygen atoms cluster with NO_3^- at the same collision-limited rate as gaseous H_2SO_4. Consequently, the calibration factor C derived for gaseous H_2SO_4 is applied to these multi-sulfur species. It should be noted that this assumption may introduce significant uncertainties in the quantification of multi-sulfur species, due to the sensitivity difference between multi-sulfur species and H_2SO_4.

Text S6. Box-model description for the reaction pathways of RO_2• in the DMS + •OH experiment

A zero-dimensional photochemical box model was constructed to characterize the fate of peroxy radicals formed during DMS oxidation under NO_x-free chamber conditions. The model simulates the

temporal evolution of •OH, HO_2•, and RO_2• and evaluates the relative importance of termination pathways of RO_2• + HO_2• and RO_2• + RO_2• (Lightfoot et al., 1992; Orlando and Tyndall, 2012). The objective is mechanistic interpretation of radical fate rather than explicit prediction of product distributions. Therefore, subsequent oxidation of stabilized products was not represented. •OH production follows an effective PAM framework in which ozone photolysis generates $O(^1D)$, followed by rapid •OH formation (Table S2) (Atkinson et al., 2004; Lambe et al., 2011). DMS oxidation is initiated by •OH via H-abstraction and •OH-addition pathways (Jacob et al., 2023; Saunders et al., 2003). Although listed separately in Table S2, their resulting peroxy radicals were treated within a condensed RO_2• scheme to focus on RO_2• fate.

Rate coefficients for DMS + •OH initiation and key RO_x reactions were adopted from evaluated kinetic mechanisms (MCM v3.3.1 and related updates) and evaluated at 291 K (Table S2) (Jacob et al., 2023; Jenkin et al., 2015; Saunders et al., 2003). Under NO_x-free conditions, RO_2• loss is dominated by bimolecular reactions with HO_2• and other RO_2• radicals (Lightfoot et al., 1992; Orlando and Tyndall, 2012), these two pathways are explicitly included as the competing RO_2• termination channels presented in Figure S8. Possible intramolecular RO_2• rearrangement is represented as a transfer between RO_2• and an isomerized pool ($R'O_2$) for bookkeeping purposes only, both pools undergo identical RO_2• + HO_2• and RO_2• + RO_2• reactions (Crounse et al., 2013; Jacob et al., 2023). Stabilized products formed from RO_2• termination reactions (e.g., ROOH and carbonyl-type products) are treated as inert end products. Because HO_2• regulates RO_2• fate under low-NO_x conditions, the HO_2• self-reaction (HO_2• + HO_2• → H_2O_2 + O_2) is included as a fundamental HO_2• sink (Atkinson et al., 2004; Lightfoot et al., 1992). A first-order dilution and wall loss term (0.02752 min^{-1}) is applied uniformly to represent chamber losses.

Figure S7 shows simulated DMS, •OH, HO_2•, and RO_2• concentrations over the first 6 min. Figure S8 presents the instantaneous fractional contributions of RO_2• + RO_2• and RO_2• + HO_2• to total RO_2• termination. After an initial transient period, the system approaches quasi-steady radical behavior, and the relative contributions of the two termination channels remain approximately constant. The complete reaction set and kinetic parameters are summarized in Table S2.

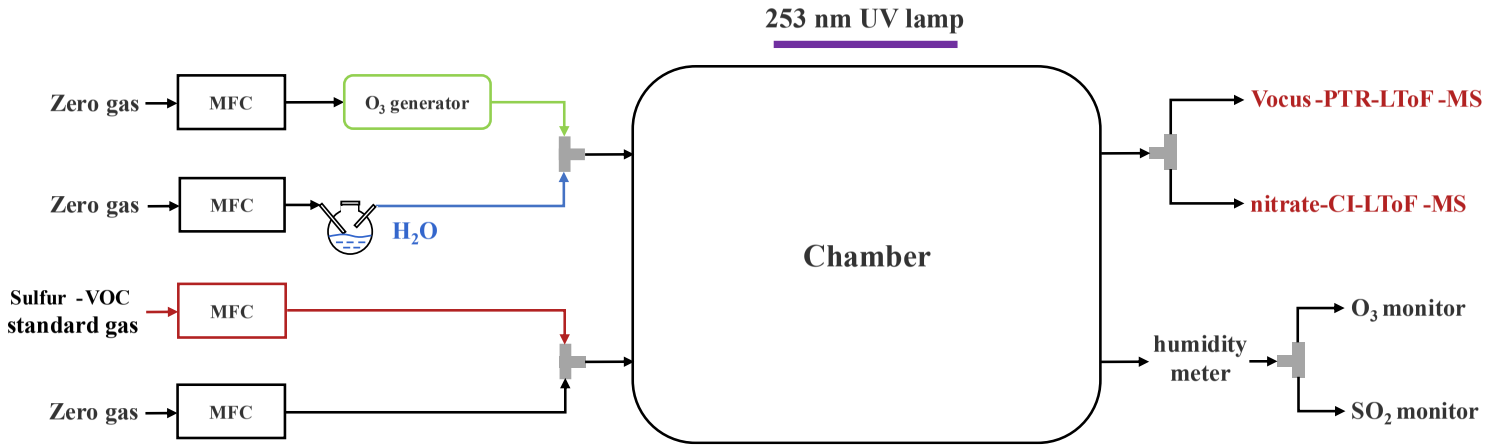

Figure S1. A scheme of the chamber set-up and instruments used in the laboratory experiments. MFC: mass flow controller.

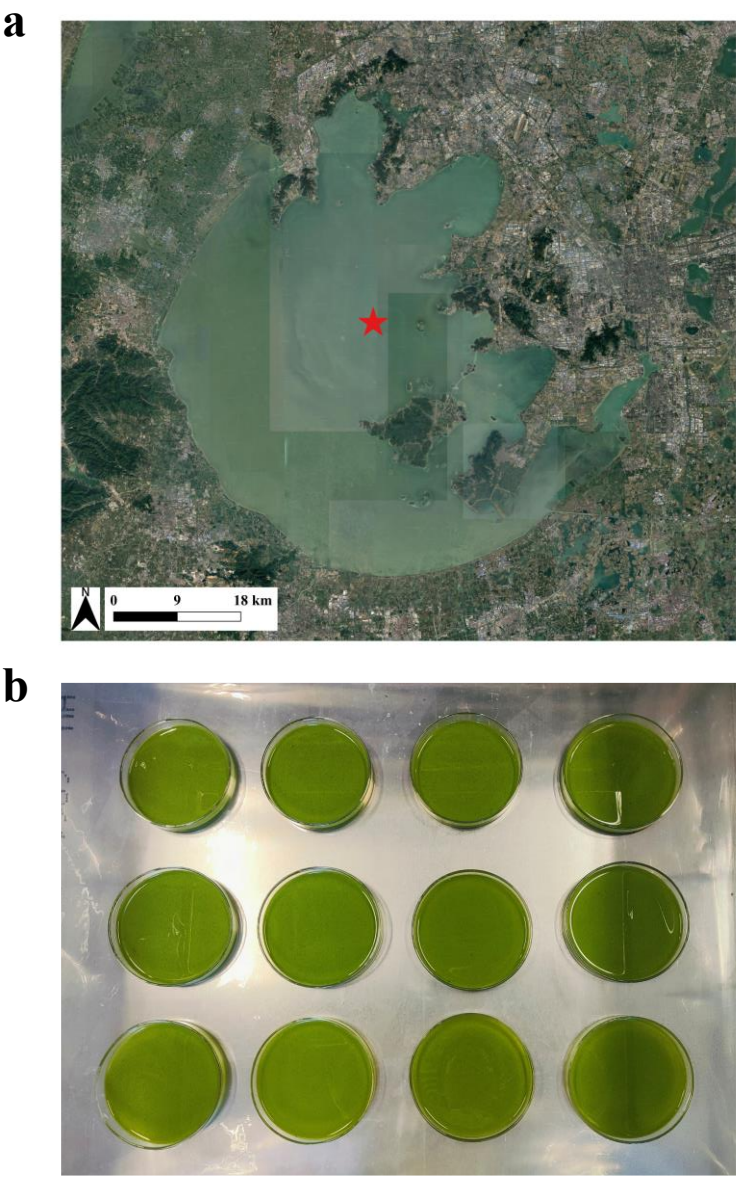

Figure S2. (a) Satellite image revised from © Google Maps of Taihu Lake, China. The red star marks the central lake region. The scale bar indicates distance in kilometers. (b) Schematic diagram of freshwater algae samples in Petri dishes placed in the chamber for static incubation.

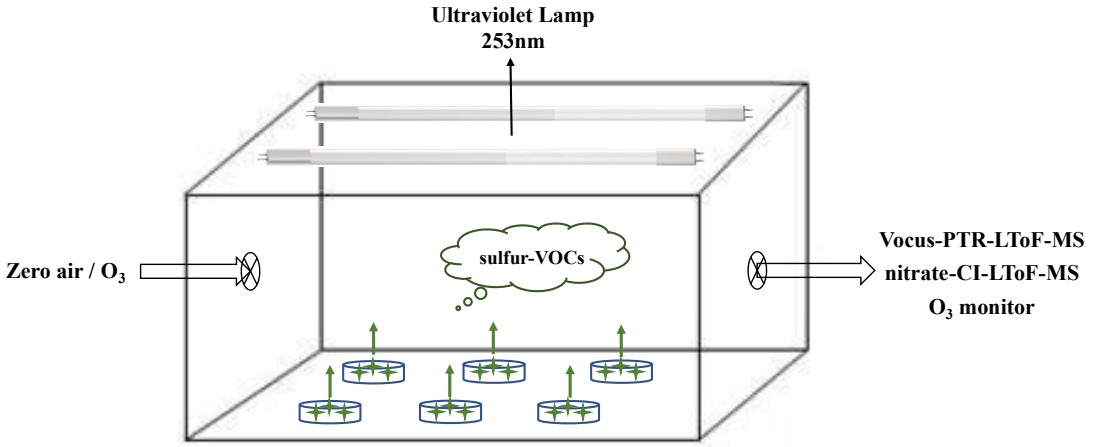

123

124 **Figure S3.** Schematic diagram of the chamber for the emission characterization of freshwater algae,
125 showing the main chamber (100 cm (L)×86 cm (W)×62 cm (H), volume 533 L) with algae water samples.

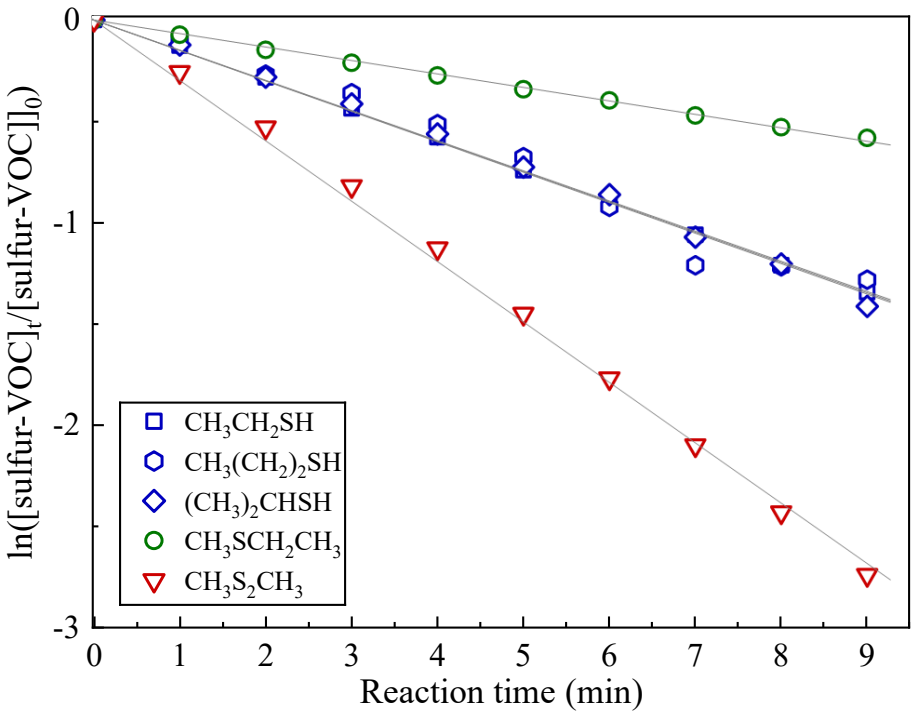

126

127 **Figure S4.** Plots of *ln*([sulfur-VOC]$_t$/[sulfur-VOC]$_0$) versus reaction time for •OH-initiated decay of
128 ethanethiol (CH_3CH_2SH), 1-propanethiol ($CH_3(CH_2)_2SH$), 2-propanethiol ($(CH_3)_2CHSH$), methyl
129 ethyl sulfide ($CH_3SCH_2CH_3$) and dimethyl disulfide ($CH_3S_2CH_3$).

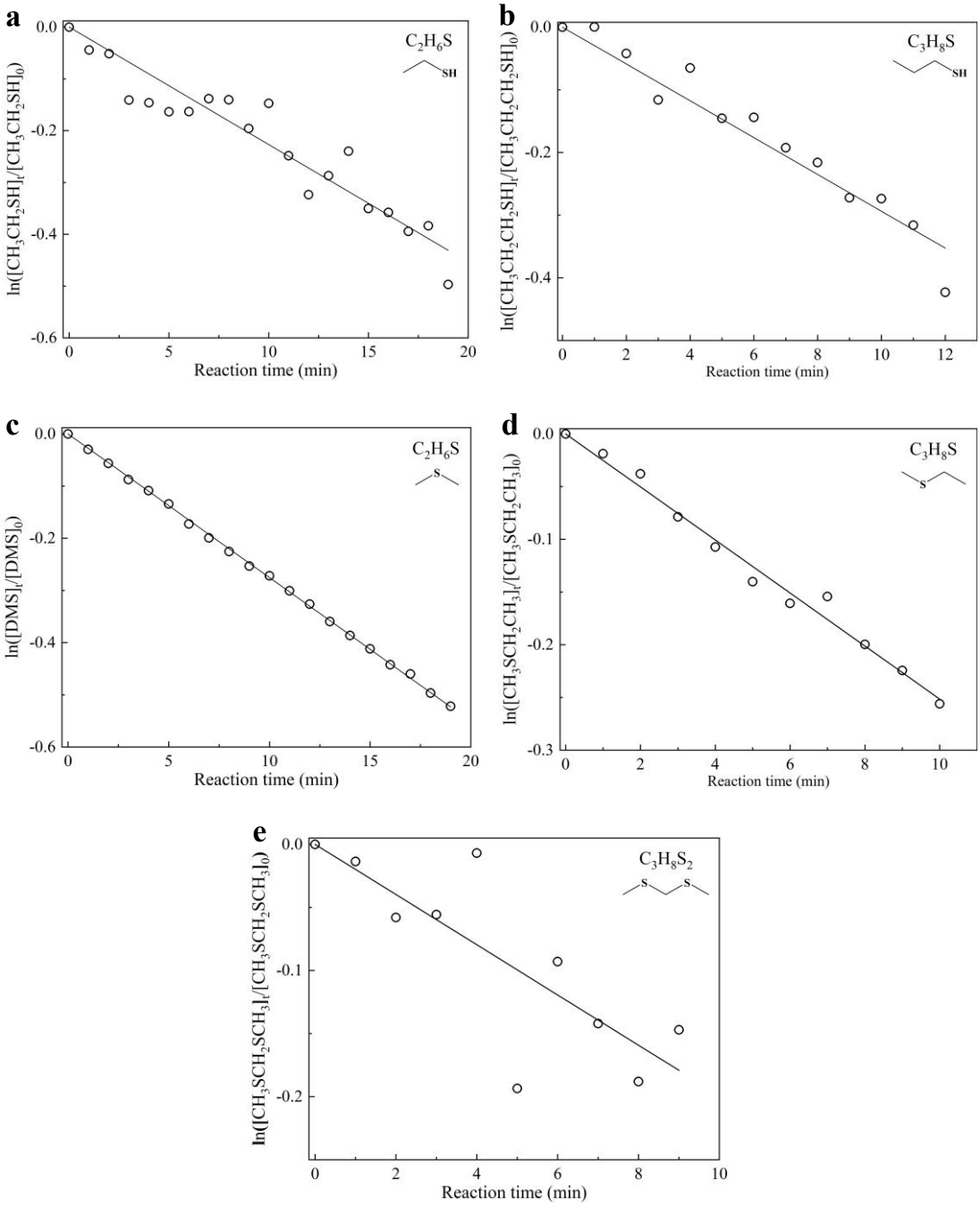

Figure S5. Plots of *ln*([sulfur-VOC]$_t$/[sulfur-VOC]$_0$) versus reaction time for the estimation of wall loss and dilution loss of sulfur-VOCs. Panels (a-e) correspond to ethanethiol (C_2H_6S), 1-propanethiol (C_3H_8S), dimethyl sulfide (C_2H_6S), methyl ethyl sulfide (C_3H_8S) and bis(methylthio)methane ($C_3H_8S_2$), respectively.

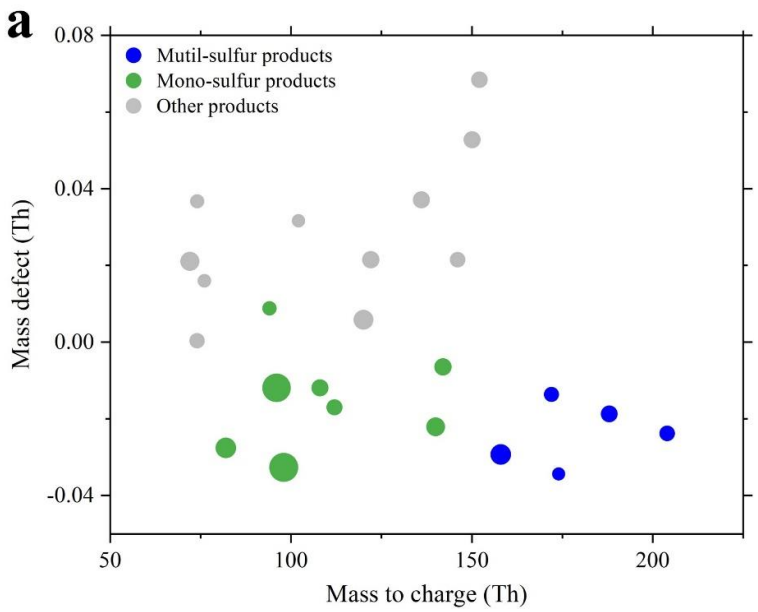
a
Mutil-sulfur products
Mono-sulfur products
Other products
Mass defect (Th)
Mass to charge (Th)
0.08
0.04
0.00
-0.04
50
100
150
200

137

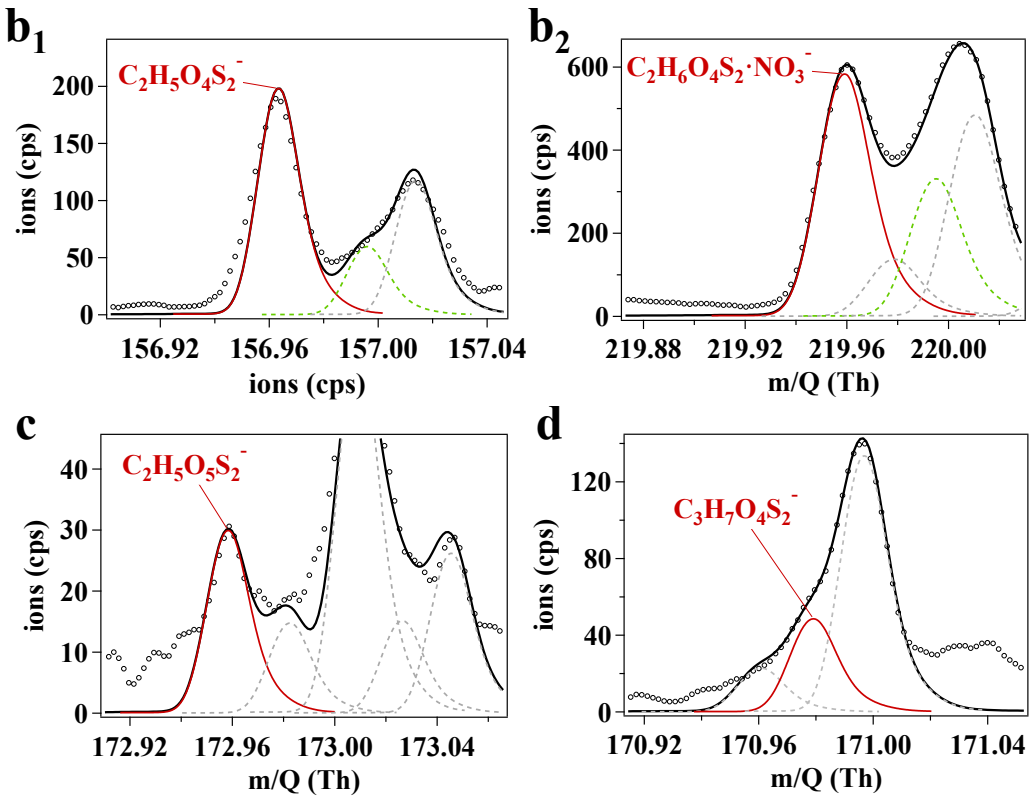
b1
C2H5O4S2-
ions (cps)
156.92
156.96
157.00
157.04
b2
C2H6O4S2·NO3-
ions (cps)
m/Q (Th)
219.88
219.92
219.96
220.00
c
C2H5O5S2-
ions (cps)
m/Q (Th)
172.92
172.96
173.00
173.04
d
C3H7O4S2-
ions (cps)
m/Q (Th)
170.92
170.96
171.00
171.04

138

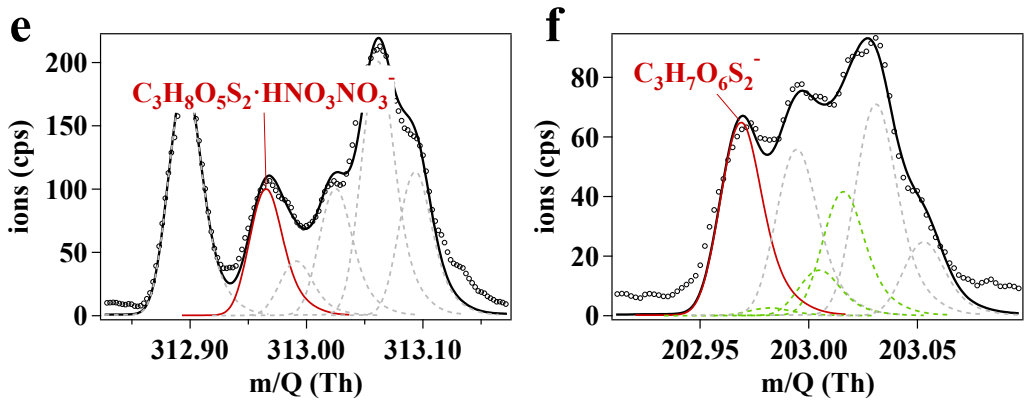

139

140 **Figure S6.** (a) Mass defect plot of reaction products formed from the •OH-initiated oxidation of DMS
141 detected by nitrate-CI-ToF-MS. Blue markers denote multi-sulfur products, green markers indicate
142 mono-sulfur products, and gray markers represent other products. (b-f) High-resolution peak fitting plots
143 of the identified multi-sulfur products.

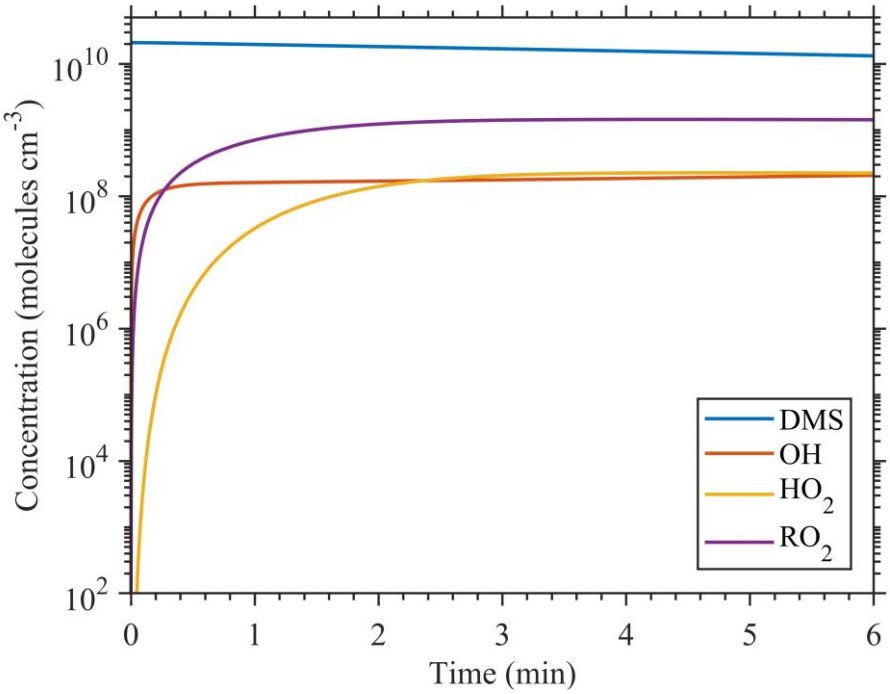

Figure S7. Time series of simulated DMS, •OH, HO_2•, and RO_2• concentrations in the chamber under NO_x-free conditions (Exp.10 in Table 1). The model represents DMS oxidation initiated by •OH over the first 6 min of the experiment.

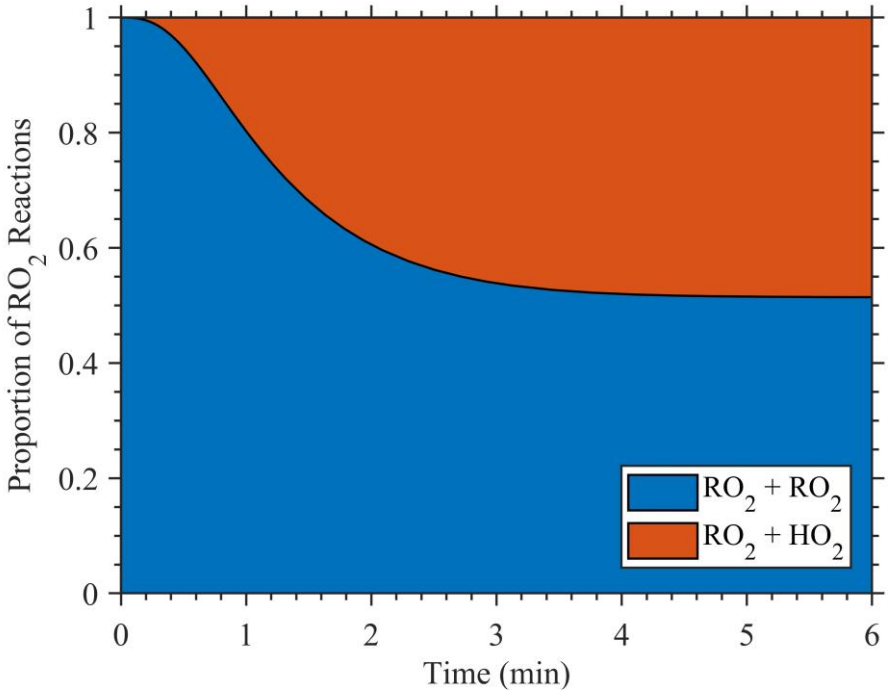

Figure S8. Simulated RO_2• termination pathways during DMS oxidation under NO_x-free conditions (Exp.10 in Table 1). The stacked area plot shows the fractional contributions of RO_2• + RO_2• and RO_2• + HO_2• reactions to total RO_2• termination as a function of reaction time over the first 6 min.

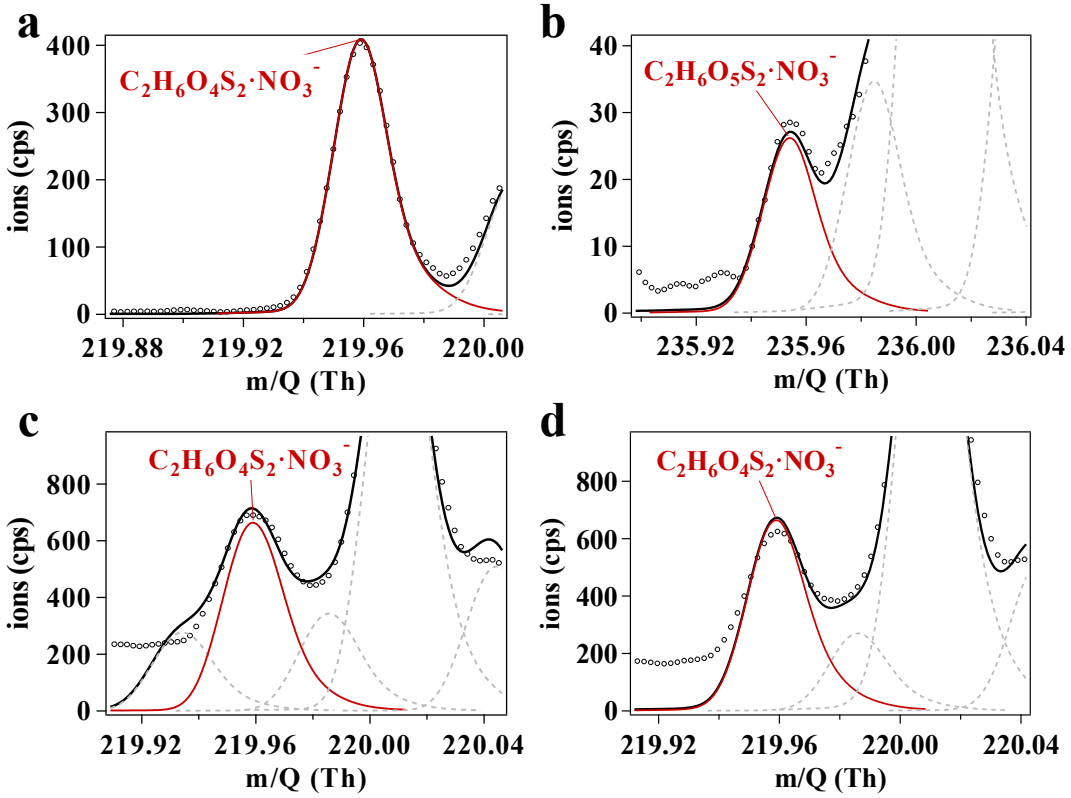

Figure S9. High-resolution peak fitting plots of multi-sulfur products formed from the •OH-initiated oxidation of sulfides ($CH_3SCH_2CH_3$ (panel a-b), $CH_3SCH_2SCH_3$ (panel c) and $CH_3S_2CH_3$ (panel d)).

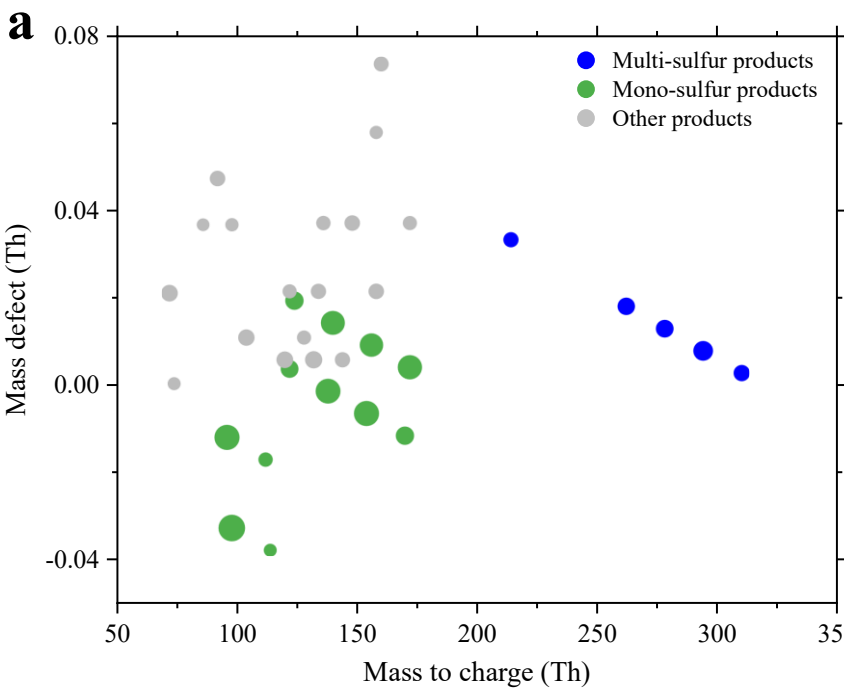
a
Multi-sulfur products
Mono-sulfur products
Other products
Mass defect (Th)
Mass to charge (Th)
0.08
0.04
0.00
-0.04
50
100
150
200
250
300
35

156

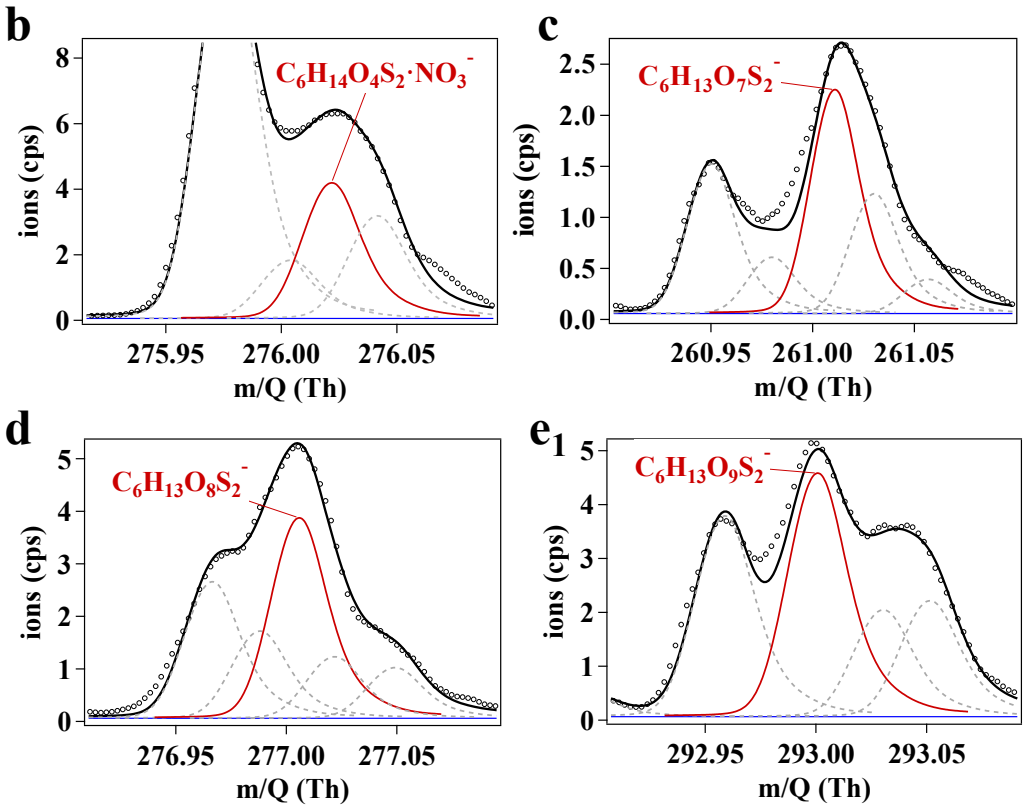
b
$C_6H_{14}O_4S_2 \cdot NO_3^-$
ions (cps)
m/Q (Th)
c
$C_6H_{13}O_7S_2^-$
d
$C_6H_{13}O_8S_2^-$
e1
$C_6H_{13}O_9S_2^-$

157

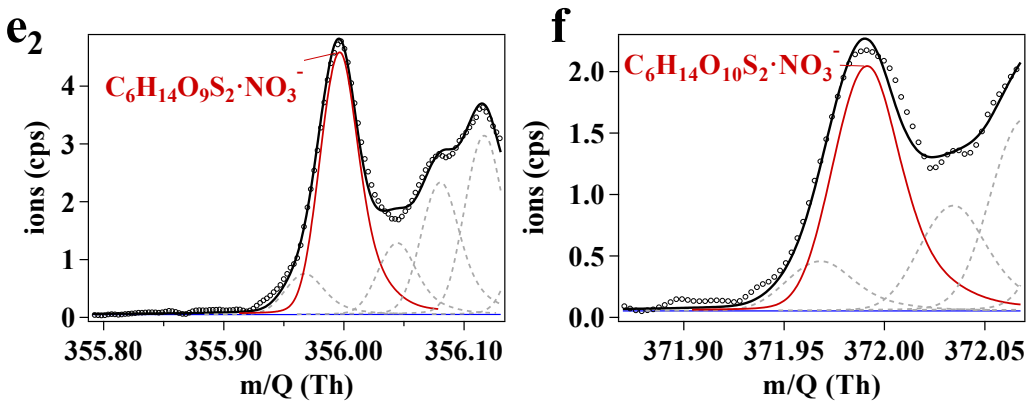

158

159 **Figure S10.** (a) Mass defect plot of reaction products formed from the •OH-initiated oxidation of
160 $HS(CH_2)_3SH$ detected by nitrate-CI-ToF-MS. Blue markers denote multi-sulfur products, green markers
161 indicate mono-sulfur products, and gray markers represent other products. (b-f) High-resolution peak
162 fitting plots of the identified multi-sulfur products.

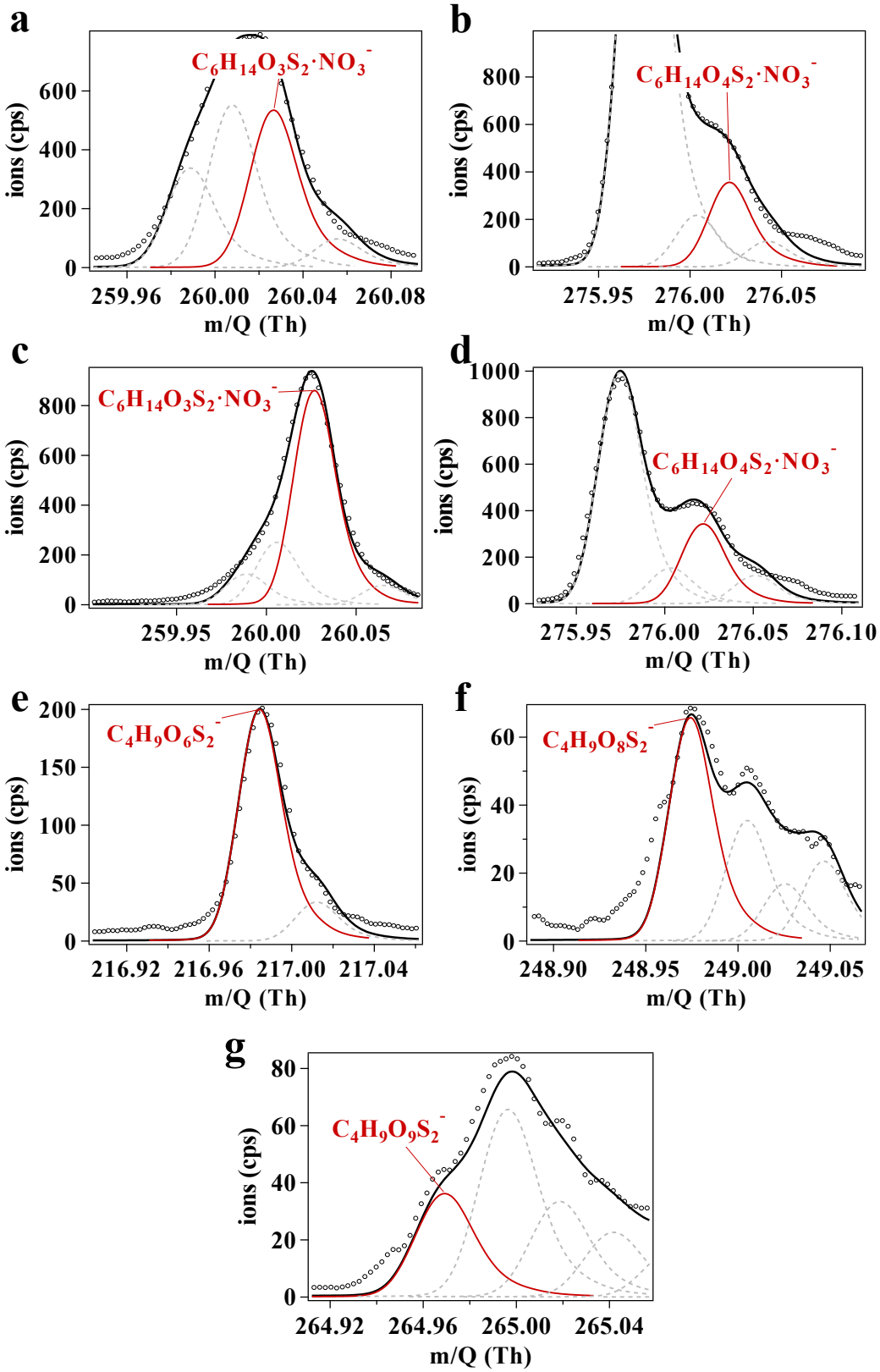

Figure S11. High-resolution peak fitting plots of multi-sulfur products formed from the •OH-initiated oxidation of $CH_3(CH_2)_2SH$ (panel a-b), $(CH_3)_2CHSH$ (panel c-d) and $HS(CH_2)_2SH$ (panel e-g).

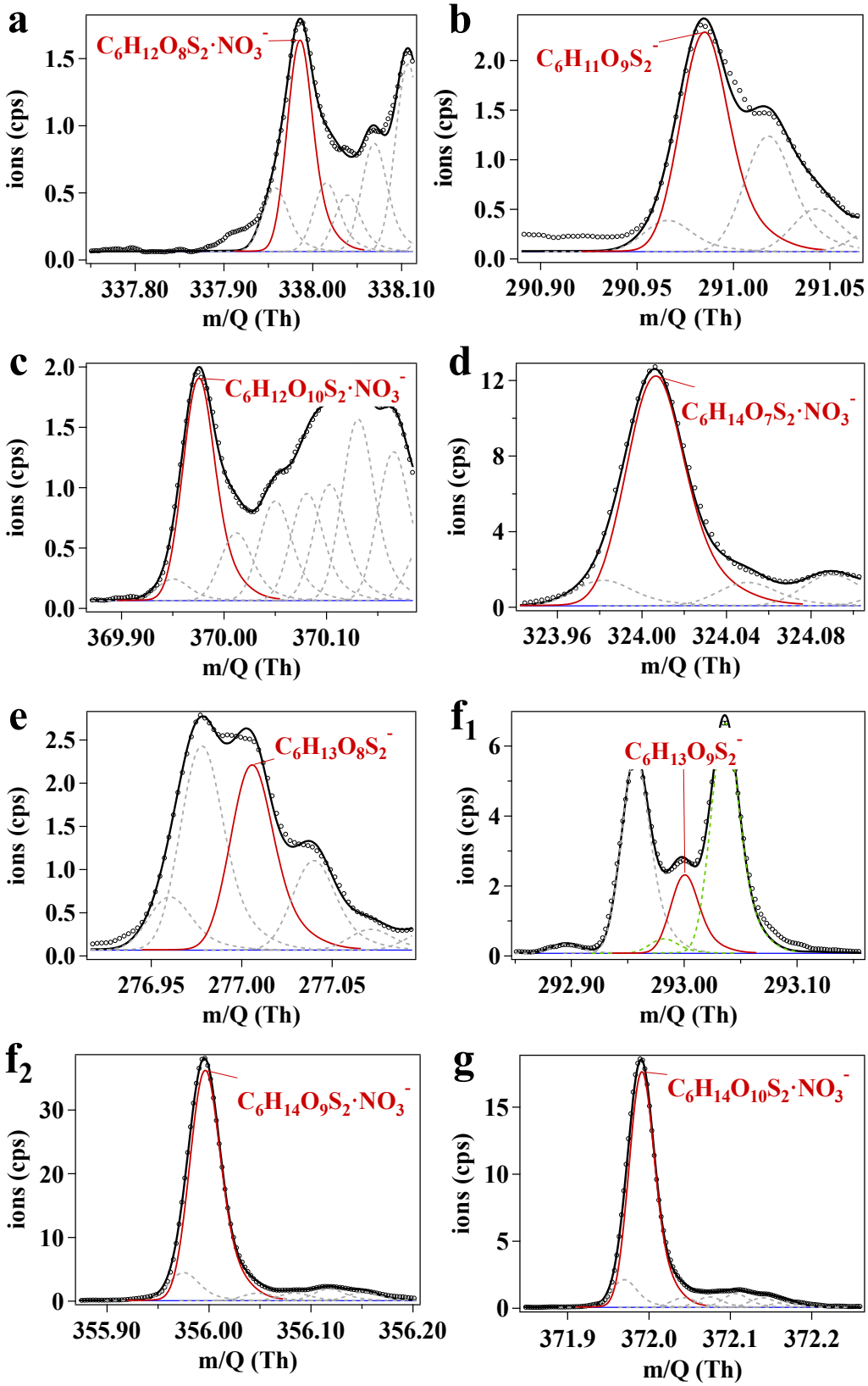

Figure S12. High-resolution peak fitting plots of multi-sulfur products formed from the •OH-initiated oxidation of cyclic sulfide (trimethylene sulfide, C_3H_6S).

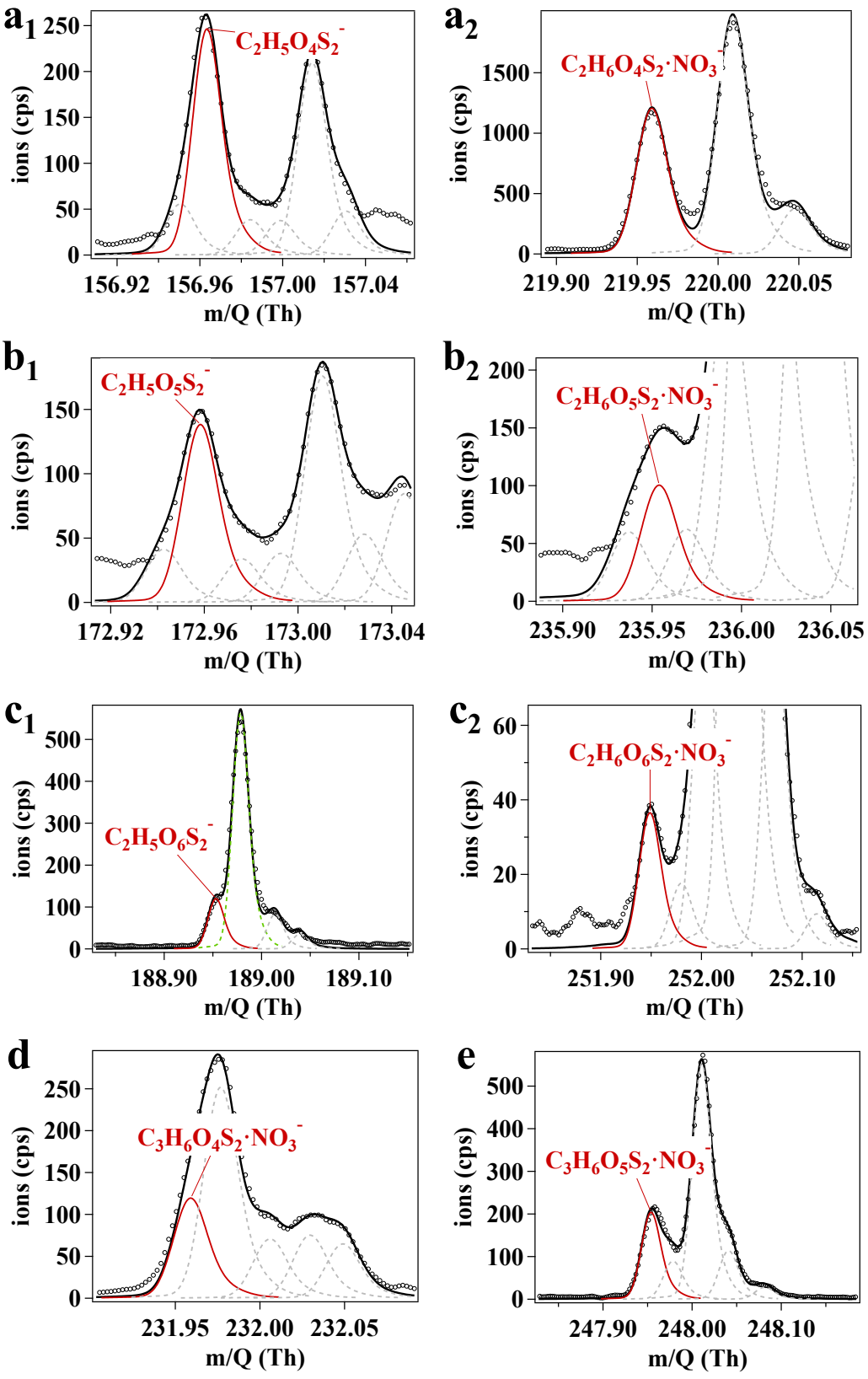
a1
C2H5O4S2-
ions (cps)
m/Q (Th)
a2
C2H6O4S2·NO3-
b1
C2H5O5S2-
b2
C2H6O5S2·NO3-
c1
C2H5O6S2-
c2
C2H6O6S2·NO3-
d
C3H6O4S2·NO3-
e
C3H6O5S2·NO3-

173

174

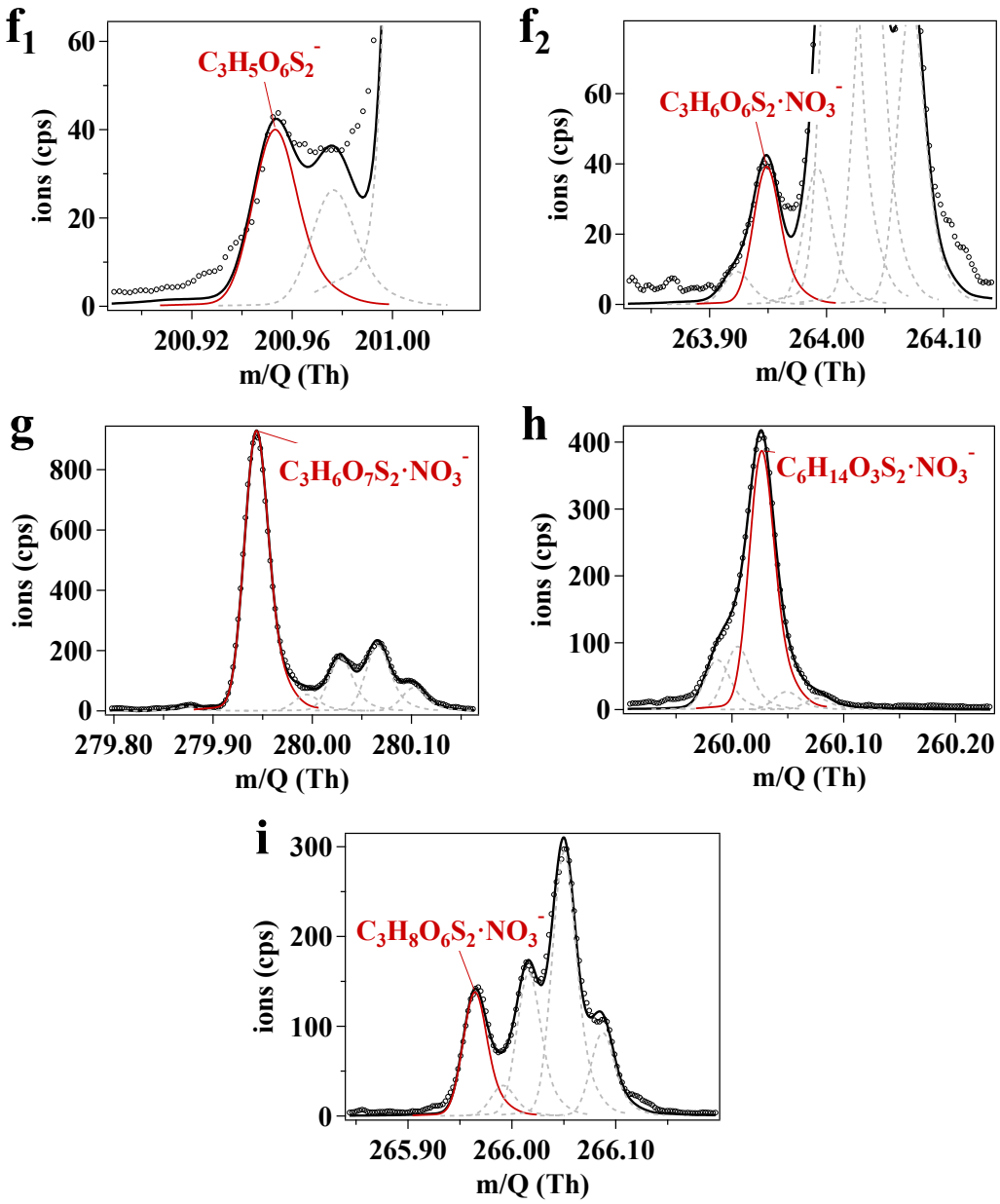

175

176 **Figure S13.** High-resolution peak fitting plots of multi-sulfur products formed from the •OH-initiated

177 oxidation of cyclic sulfide (1,3-dithiolane, $C_3H_6S_2$).

178

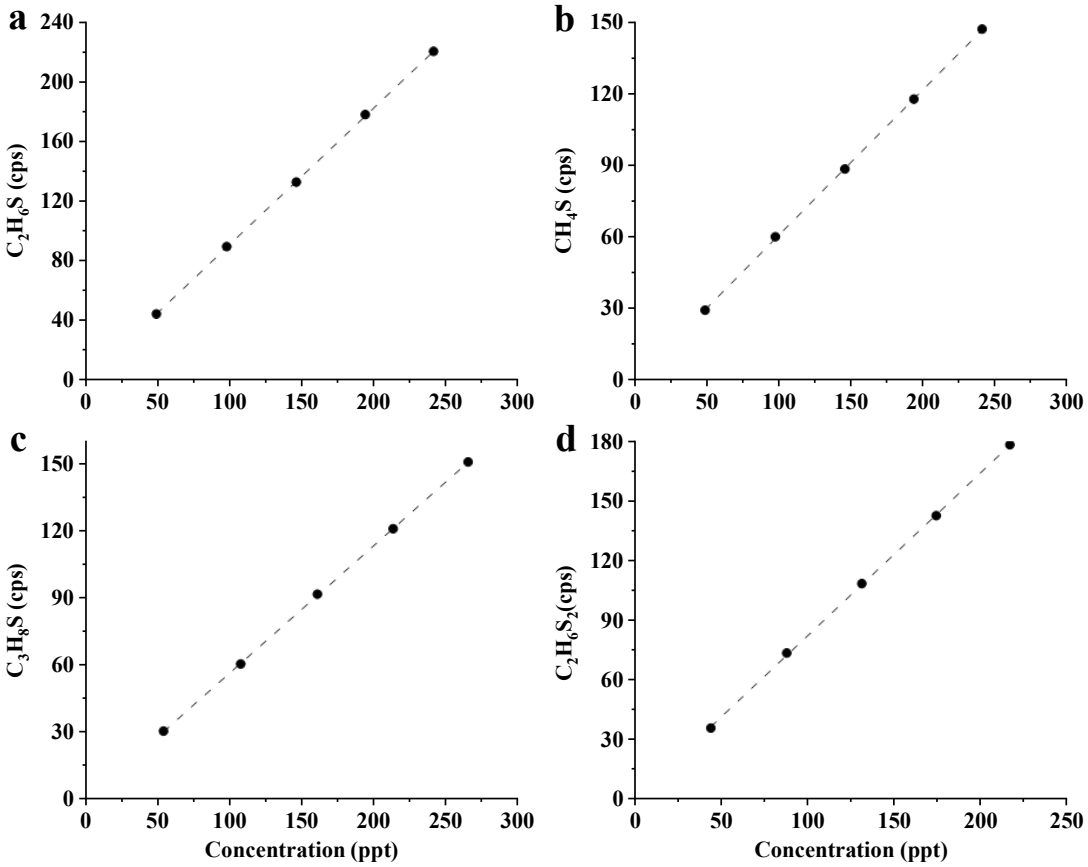

Figure S14. Calibration curves relating instrument signal (cps) to standard mixing ratio (ppt) for the target sulfur-VOCs measured by Vocus-PTR-LToF-MS, including (a) C_2H_6S, (b) CH_4S, (c) C_3H_8S, and (d) $C_2H_6S_2$. Dashed lines represent linear least-squares fits.

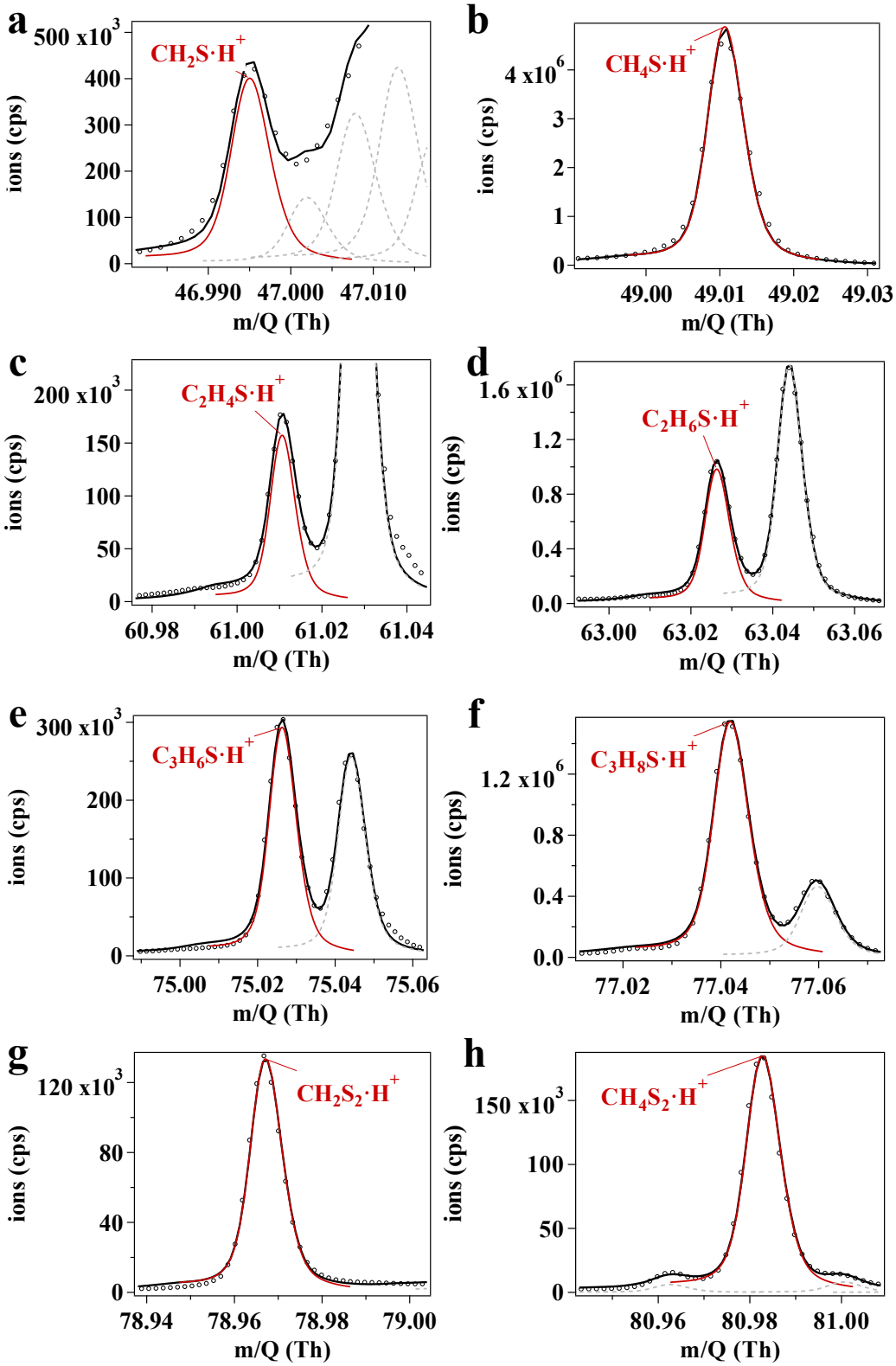
a
500 x10^3
400
300
200
100
0
ions (cps)
CH2S·H+
46.990
47.000
47.010
m/Q (Th)
b
4 x10^6
3
2
1
0
ions (cps)
CH4S·H+
49.00
49.01
49.02
49.03
m/Q (Th)
c
200 x10^3
150
100
50
0
ions (cps)
C2H4S·H+
60.98
61.00
61.02
61.04
m/Q (Th)
d
1.6 x10^6
1.2
0.8
0.4
0.0
ions (cps)
C2H6S·H+
63.00
63.02
63.04
63.06
m/Q (Th)
e
300 x10^3
200
100
0
ions (cps)
C3H6S·H+
75.00
75.02
75.04
75.06
m/Q (Th)
f
1.2 x10^6
0.8
0.4
0.0
ions (cps)
C3H8S·H+
77.02
77.04
77.06
m/Q (Th)
g
120 x10^3
80
40
0
ions (cps)
CH2S2·H+
78.94
78.96
78.98
79.00
m/Q (Th)
h
150 x10^3
100
50
0
ions (cps)
CH4S2·H+
80.96
80.98
81.00
m/Q (Th)

183

184

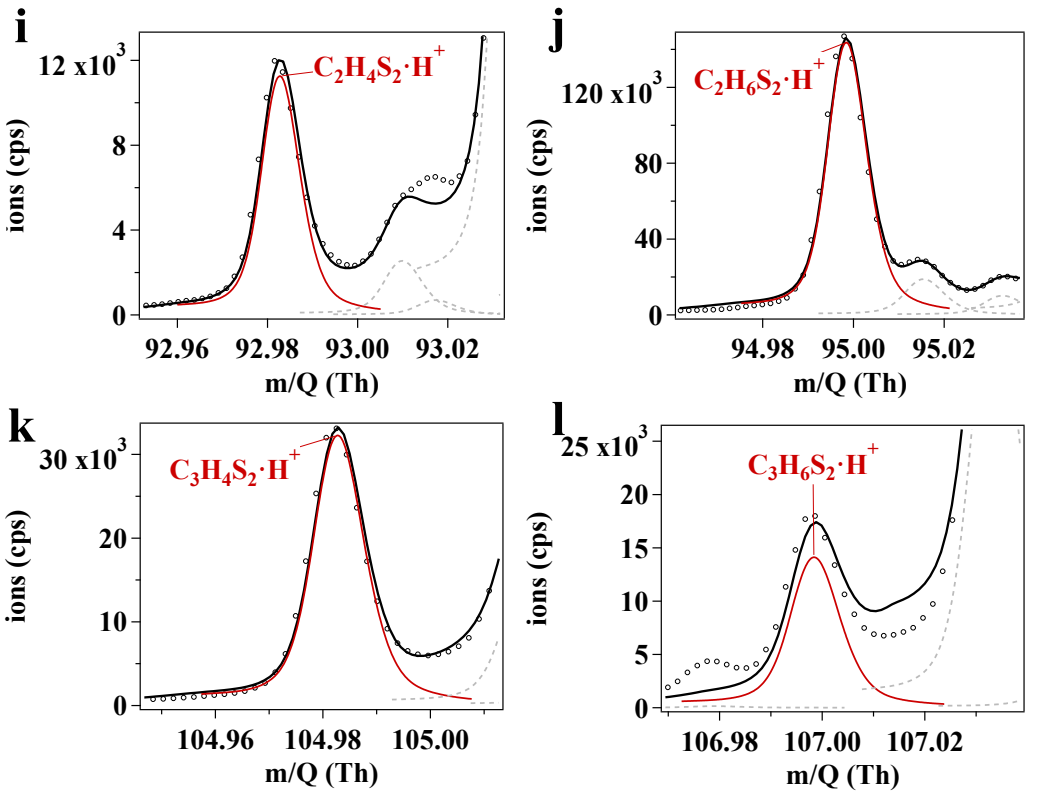
i
12 x10^3
8
4
0
ions (cps)
C2H4S2·H+
92.96
92.98
93.00
93.02
m/Q (Th)
j
120 x10^3
80
40
0
ions (cps)
C2H6S2·H+
94.98
95.00
95.02
m/Q (Th)
k
30 x10^3
20
10
0
ions (cps)
C3H4S2·H+
104.96
104.98
105.00
m/Q (Th)
l
25 x10^3
20
15
10
5
0
ions (cps)
C3H6S2·H+
106.98
107.00
107.02
m/Q (Th)

185

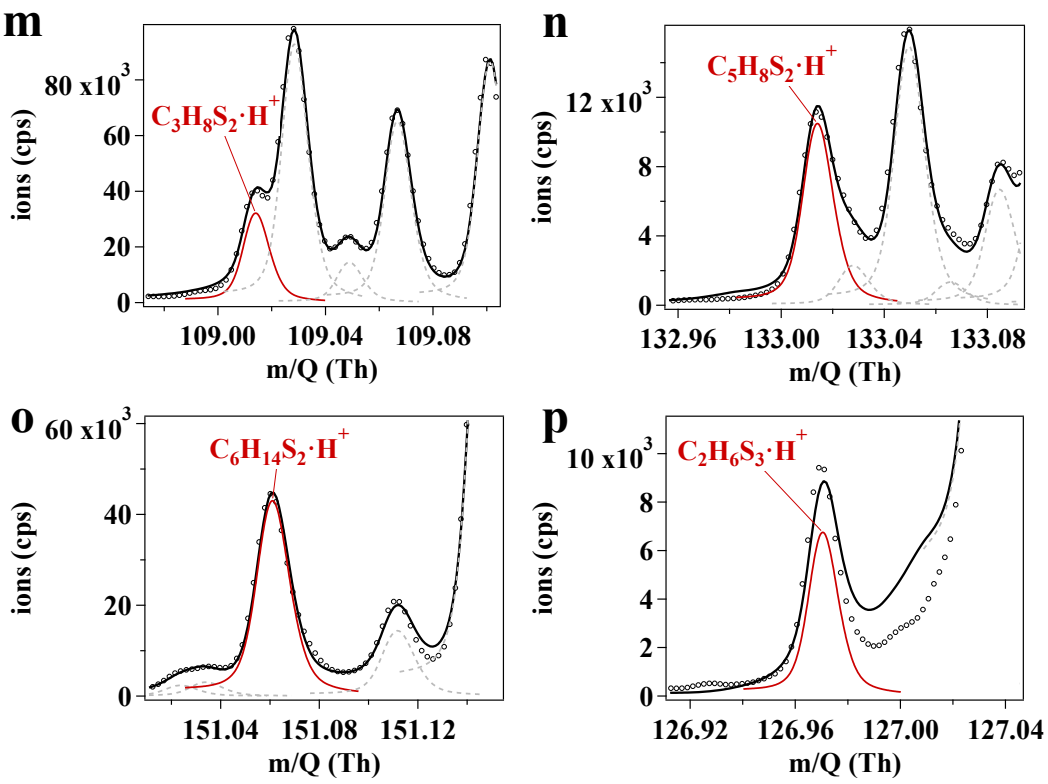
m
80 x10^3
60
40
20
0
ions (cps)
C3H8S2·H+
109.00
109.04
109.08
m/Q (Th)
n
12 x10^3
8
4
0
ions (cps)
C5H8S2·H+
132.96
133.00
133.04
133.08
m/Q (Th)
o
60 x10^3
40
20
0
ions (cps)
C6H14S2·H+
151.04
151.08
151.12
m/Q (Th)
p
10 x10^3
8
6
4
2
0
ions (cps)
C2H6S3·H+
126.92
126.96
127.00
127.04
m/Q (Th)

186

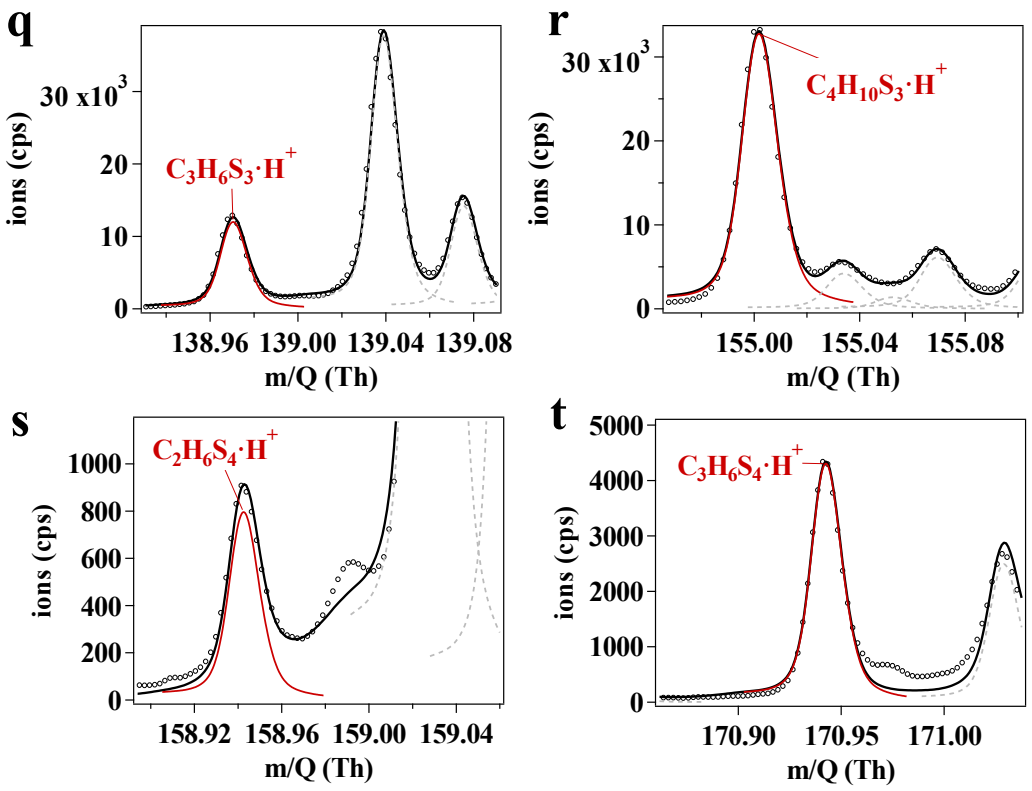

187

188 **Figure S15.** (a-t) High-resolution peak fitting plots of 20 sulfur- VOCs emitted from freshwater algae

189 and detected by Vocus-PTR-LToF-MS.

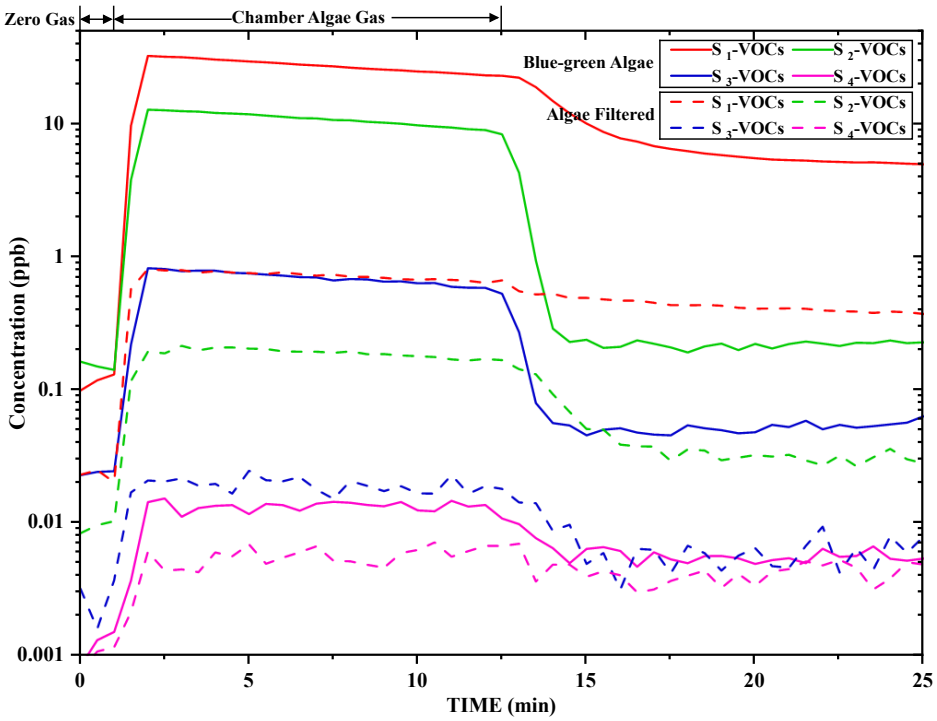

Figure S16. Inter-comparison of the concentrations of sulfur-VOCs between freshwater algae samples and samples with algae filtered by glass fiber filter. The 20 sulfur-VOCs are classified into four groups ($S_{1\text{-}4}$-VOCs) based on the number of sulfur atoms in their chemical formulas.

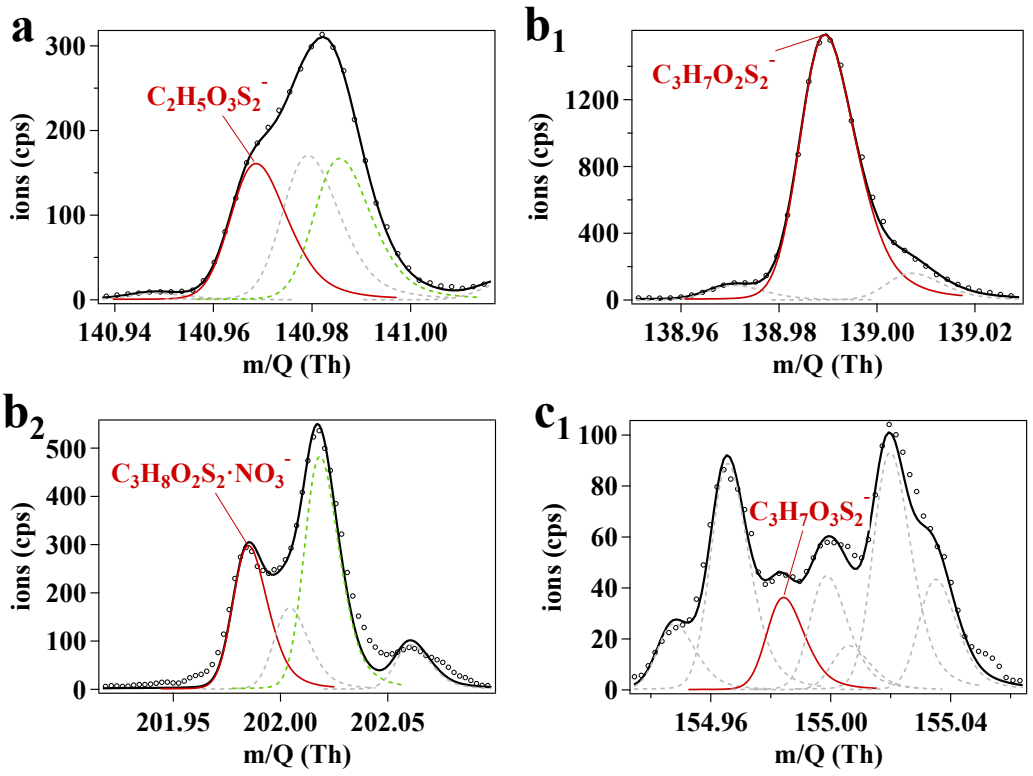
a
$C_2H_5O_3S_2^-$
ions (cps)
m/Q (Th)
b1
$C_3H_7O_2S_2^-$
b2
$C_3H_8O_2S_2 \cdot NO_3^-$
c1
$C_3H_7O_3S_2^-$
c2
$C_3H_8O_3S_2 \cdot NO_3^-$
d
$C_3H_7O_2S_3^-$
e
$C_3H_8O_3S_3 \cdot NO_3^-$
f
$C_4H_9O_2S_2^-$

194

195

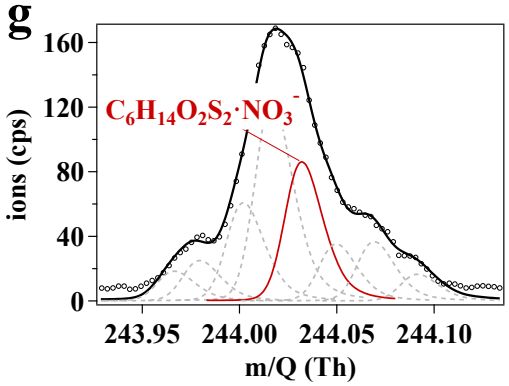

196

197 **Figure S17.** High-resolution peak fitting plots of 7 multi-sulfur products detected by nitrate-CI-ToF-
198 MS in the freshwater algae chamber experiments, whose molecular formulas could be deduced from
199 sulfur-VOCs chamber simulation experiments.

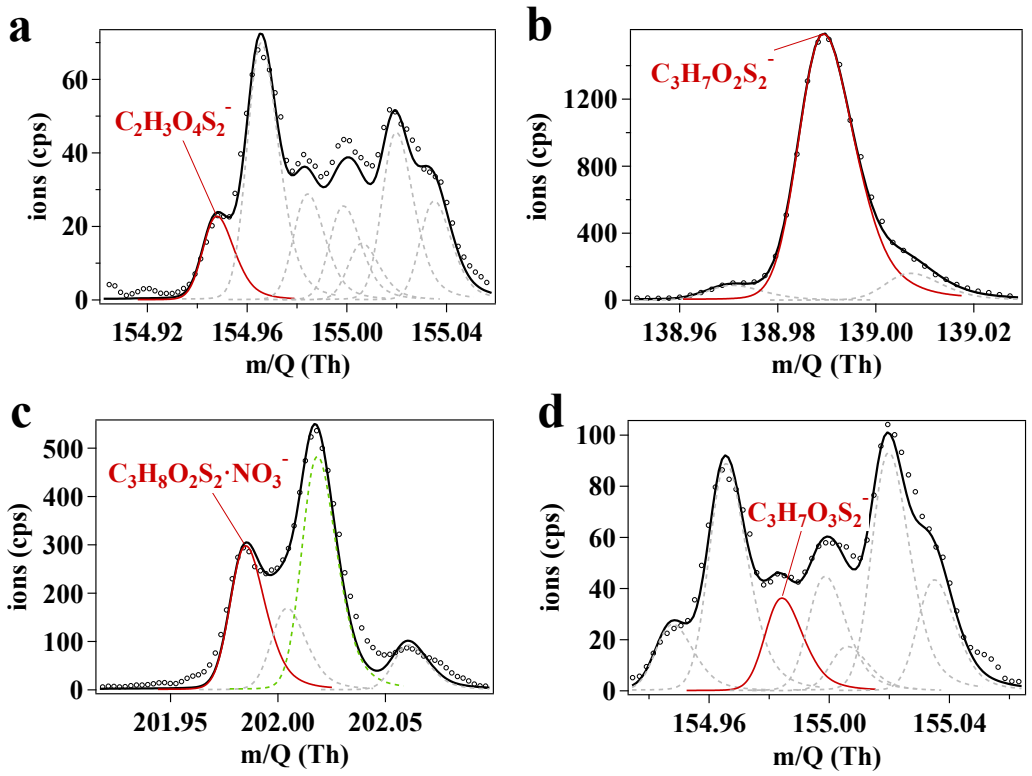

Figure S18. High-resolution peak fitting plots of 4 multi-sulfur products detected by nitrate-CI-ToF-MS in the freshwater algae chamber experiments, whose molecular formulas cannot be deduced from sulfur-VOCs chamber simulation experiments.

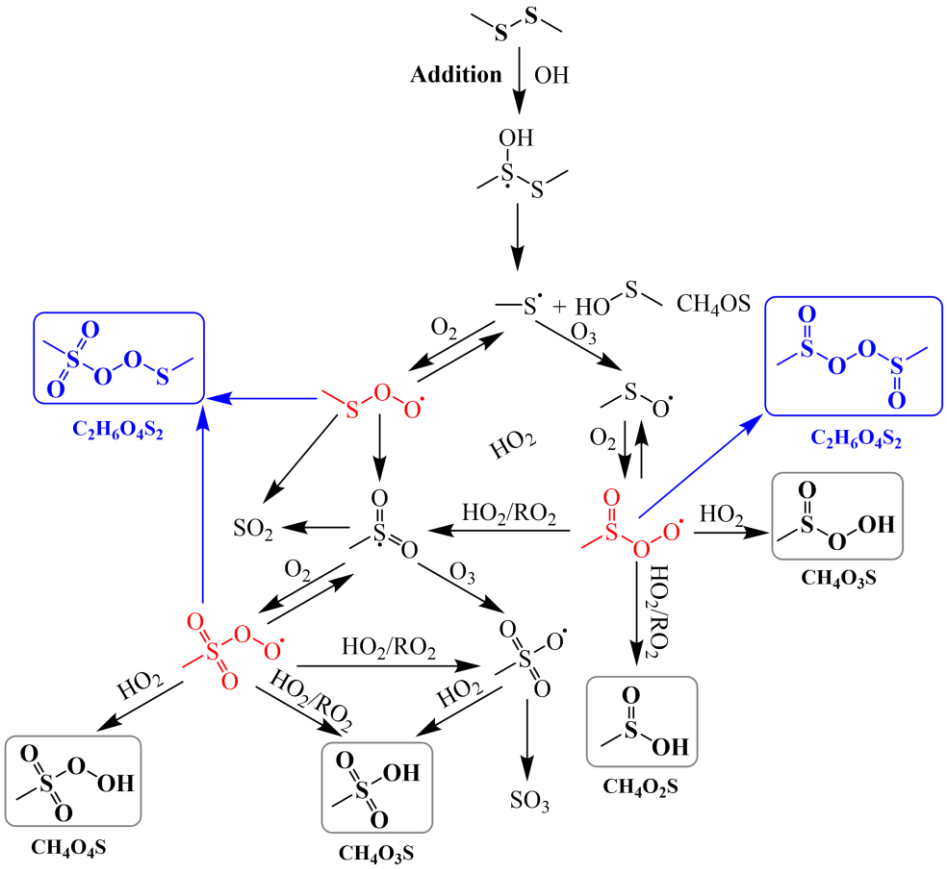

Scheme S1. Scheme of the reaction pathways of DMDS with •OH.

207 **Table S1.** Specifications of sulfur-VOCs investigated in our study.

Serial number	Reagent name	CAS number	Physical state	Brand owner	Product number	Purity
1	ethanethiol	75-08-1	liquid	Sigma-Aldrich	E3708	97%
2	1-propanethiol	107-03-9	liquid	Sigma-Aldrich	P50757	99%
3	2-propanethiol	75-33-2	liquid	Sigma-Aldrich	59590	⩾97%
4	1,2-ethanedithiol	540-63-6	liquid	Sigma-Aldrich	02390	⩾98.0%
5	1,3-propanedithiol	109-80-8	liquid	Sigma-Aldrich	P50609	99%
6	dimethyl sulfide	75-18-3	liquid	Sigma-Aldrich	274380	⩾99%
7	methyl ethyl sulfide	624-89-5	liquid	Sigma-Aldrich	238317	96%
8	bis(methylthio)methane	1618-26-4	liquid	Sigma-Aldrich	W387800	⩾99%
9	trimethylene sulfide	287-27-4	liquid	Macklin	T838543	98%
10	1,3-dithiolane	4829-04-3	liquid	Macklin	D920796	97%
11	dimethyl disulfide	624-92-0	liquid	Macklin	M832301	98%

208

Table S2. Reaction mechanisms were used to model the fate of RO_2• generated from •OH-initiated oxidation of DMS under NO_x-free chamber conditions at 291 K (Exp.10 in Table 1). The number in front of the product indicates the yield of the product.

Reactant 1	Reactant 2	Product	Rate Coeff	Citation
O_3	hv	$O(^1D)$	1.00E-05	a
$O(^1D)$		2OH	2.00E+02	a
DMS	OH	RO_2_MSP	4.74E-12	b
RO_2_MSP	O_2	RO_2_HPMTF	3.61E-02	c
RO_2_MSP		RO_2_SO	1.00E-02	d
RO_2_SO	O_2	RO_2_SOO	5.00E-02	d
RO_2_SOO	O_2	RO_2_SO_2	2.00E-01	d
RO_2_MSP	HO_2	P	2.54E-11	e
RO_2_HPMTF	HO_2	P	1.66E-11	c
RO_2_SO	HO_2	P	2.54E-11	e
RO_2_SOO	HO_2	P	2.54E-11	e
RO_2_SO_2	HO_2	P	2.54E-11	e
RO_2_MSP	RO_2_MSP	2RO	4.00E-12	f
RO_2_MSP	RO_2_HPMTF	2RO	2.28E-12	f
RO_2_MSP	RO_2_SO	2RO	6.32E-12	f
RO_2_MSP	RO_2_SOO	2RO	6.32E-12	f
RO_2_MSP	RO_2_SO_2	2RO	6.32E-12	f
RO_2_HPMTF	RO_2_HPMTF	2RO	1.30E-12	f
RO_2_HPMTF	RO_2_SO	2RO	3.61E-12	f
RO_2_HPMTF	RO_2_SOO	2RO	3.61E-12	f
RO_2_HPMTF	RO_2_SO_2	2RO	3.61E-12	f
RO_2_SO	RO_2_SO	2RO	1.00E-11	f
RO_2_SO	RO_2_SOO	2RO	1.00E-11	f
RO_2_SO	RO_2_SO_2	2RO	1.00E-11	f
RO_2_SOO	RO_2_SOO	2RO	1.00E-11	f
RO_2_SOO	RO_2_SO_2	2RO	1.00E-11	f
RO_2_SO_2	RO_2_SO_2	2RO	1.00E-11	f
RO		HO_2	5.00E+00	d
HO_2	HO_2	P	3.00E-12	g

a PAM/OFR photochemical framework for OH generation using effective photolysis and O(1D)→OH conversion parameters (Lambe et al., 2011).

b Gas-phase OH abstraction of DMS forming CH_3SCH_2OO, rate expression from (Saunders et al., 2003).

c DMS abstraction oxidation chain and RO_2_HPMTF chemistry following the mechanism summarized in (Jacob et al., 2023).

d Lumped first-order oxidation and RO-to-HO_2 conversion steps introduced to represent multi-step oxidation and maintain HO_x closure in chamber box models (following common box-model practice (Jacob et al., 2023; Lambe et al., 2011).

e Generic $RO_2 + HO_2$ termination rate expression adopted from the Master Chemical Mechanism (Jenkin et al., 2015).

f $RO_2 + RO_2$ termination parameterized using self-reaction rate constants and geometric-mean approximation for cross reactions, commonly used when explicit data are unavailable (Jacob et al., 2023; Jenkin et al., 2015).

g $HO_2 + HO_2$ termination rate from kinetic evaluations summarized by (Atkinson et al., 2004).

Notes: RO_2_MSP, RO_2_HPMTF, RO_2_SO, RO_2_SOO, and RO_2_SO_2 represent lumped classes of organic peroxy radicals formed during the oxidation of dimethyl sulfide (DMS). RO_2_MSP corresponds to the initial carbon-centered peroxy radical (e.g., $CH_3SCH_2OO•$) formed via H-abstraction. RO_2_HPMTF represents peroxy radicals formed following isomerization (e.g., $HOOCH_2SCH_2OO•$). RO_2_SO, RO_2_SOO, and RO_2_SO_2 represent sulfur-centered peroxy radicals with increasing sulfur oxidation states, intended to capture progressive sulfur oxidation (e.g., $CH_3SOO•$, $CH_3S(O)OO•$, and $CH_3S(O)_2OO•$), without resolving individual molecular identities. P denotes a lumped pool of stable, non-radical oxidation products (e.g., ROOH, carbonyls, and H_2O_2) that do not further participate in HO_x or RO_2 chemistry.

Table S3. Multi-sulfur products formed from the •OH-initiated oxidation of selected sulfur-VOCs and their volatility ($log_{10}C(291K)$) and yield (%).

Species	sulfur-VOCs	Formulae	Multi-sulfur products	Product ions	$log_{10}C(291K)$	Individual and total yield (%)	
Acyclic sulfide	dimethyl sulfide	CH_3SCH_3	$C_2H_6O_4S_2$	$C_2H_5O_4S_2^-$ $C_2H_6O_4S_2 \cdot NO_3^-$	2.27	3.286	
			$C_2H_6O_5S_2$	$C_2H_5O_5S_2^-$	1.02	0.064	4.249
			$C_3H_8O_4S_2$	$C_3H_7O_4S_2^-$	2.21	0.193	
			$C_3H_8O_5S_2$	$C_3H_8O_5S_2 \cdot HNO_3NO_3^-$	1.01	0.463	
			$C_3H_8O_6S_2$	$C_3H_7O_6S_2^-$	-0.21	0.244	
	methyl ethyl sulfide	$CH_3SCH_2CH_3$	$C_2H_6O_4S_2$	$C_2H_6O_4S_2 \cdot NO_3^-$	2.27	3.536	3.869
			$C_2H_6O_5S_2$	$C_2H_6O_5S_2 \cdot NO_3^-$	1.02	0.333	
	bis(methylthio)methane	$CH_3SCH_2SCH_3$	$C_2H_6O_4S_2$	$C_2H_6O_4S_2 \cdot NO_3^-$	2.27	0.007	0.007
Disulfide	dimethyl disulfide	$CH_3S_2CH_3$	$C_2H_6O_4S_2$	$C_2H_6O_4S_2 \cdot NO_3^-$	2.27	0.069	0.069
Monothiol	1-propanethiol	$CH_3(CH_2)_2SH$	$C_6H_{14}O_3S_2$	$C_6H_{14}O_3S_2 \cdot NO_3^-$	2.68	0.001	0.001
			$C_6H_{14}O_4S_2$	$C_6H_{14}O_4S_2 \cdot NO_3^-$	1.67	0.001	
	2-propanethiol	$(CH_3)_2CHSH$	$C_6H_{14}O_3S_2$	$C_6H_{14}O_3S_2 \cdot NO_3^-$	2.68	0.271	0.398
			$C_6H_{14}O_4S_2$	$C_6H_{14}O_4S_2 \cdot NO_3^-$	1.67	0.127	
Dithiol	1,2-ethanedithiol	$HS(CH_2)_2SH$	$C_4H_{10}O_6S_2$	$C_4H_9O_6S_2^-$	-0.26	0.053	0.097
			$C_4H_{10}O_8S_2$	$C_4H_9O_8S_2^-$	-3.94	0.019	
			$C_4H_{10}O_9S_2$	$C_4H_9O_9S_2^-$	-2.70	0.024	
	1,3-propanedithiol	$HS(CH_2)_3SH$	$C_6H_{14}O_4S_2$	$C_6H_{14}O_4S_2 \cdot NO_3^-$	1.67	0.008	0.169
			$C_6H_{14}O_7S_2$	$C_6H_{13}O_7S_2^-$	-1.65	0.027	
			$C_6H_{14}O_8S_2$	$C_6H_{13}O_8S_2^-$	-2.82	0.032	
			$C_6H_{14}O_9S_2$	$C_6H_{13}O_9S_2^-$ $C_6H_{14}O_9S_2 \cdot NO_3^-$	-4.01	0.088	
			$C_6H_{14}O_{10}S_2$	$C_6H_{14}O_{10}S_2 \cdot NO_3^-$	-5.22	0.015	

Cyclic sulfide	trimethylene sulfide	C_3H_6S	$C_6H_{12}O_8S_2$	$C_6H_{12}O_8S_2 \cdot NO_3^-$	-2.82	0.082	11.729
			$C_6H_{12}O_9S_2$	$C_6H_{11}O_9S_2^-$	-4.01	0.230	
			$C_6H_{12}O_{10}S_2$	$C_6H_{12}O_{10}S_2 \cdot NO_3^-$	-5.22	0.208	
			$C_6H_{14}O_7S_2$	$C_6H_{14}O_7S_2 \cdot NO_3^-$	-1.65	1.572	
			$C_6H_{14}O_8S_2$	$C_6H_{13}O_8S_2^-$	-2.82	0.243	
			$C_6H_{14}O_9S_2$	$C_6H_{13}O_9S_2^-$ $C_6H_{14}O_9S_2 \cdot NO_3^-$	-4.01	6.541	
			$C_6H_{14}O_{10}S_2$	$C_6H_{14}O_{10}S_2 \cdot NO_3^-$	-5.22	2.853	
	1,3-dithiolane	$C_3H_6S_2$	$C_2H_6O_4S_2$	$C_2H_5O_4S_2^-$ $C_2H_6O_4S_2 \cdot NO_3^-$	2.27	0.191	
			$C_2H_6O_5S_2$	$C_2H_5O_5S_2^-$ $C_2H_6O_5S_2 \cdot NO_3^-$	1.02	0.033	
			$C_2H_6O_6S_2$	$C_2H_5O_6S_2^-$	-0.25	0.047	
			$C_3H_6O_4S_2$	$C_3H_6O_4S_2 \cdot NO_3^-$	2.21	0.035	0.925
			$C_3H_6O_5S_2$	$C_3H_6O_5S_2 \cdot NO_3^-$	1.01	0.065	
			$C_3H_6O_6S_2$	$C_3H_5O_6S_2^-$ $C_3H_6O_6S_2 \cdot NO_3^-$	-0.21	0.025	
			$C_3H_6O_7S_2$	$C_3H_6O_7S_2 \cdot NO_3^-$	-1.46	0.335	
			$C_6H_{14}O_3S_2$	$C_6H_{14}O_3S_2 \cdot NO_3^-$	2.68	0.145	
			$C_3H_8O_6S_2$	$C_3H_8O_6S_2 \cdot NO_3^-$	-0.21	0.050	

239 **Table S4.** Molecular formulas and molecular masses of 20 sulfur-VOCs emitted from freshwater algae.

Serial number	Molecular formula	Molecular mass	Number of sulfur atoms	Concentration (ppbv)
1	CH_2S	45.9877	1	4.087
2	CH_4S	48.0033	1	11.773
3	C_2H_4S	60.0033	1	3.573
4	C_2H_6S	62.0190	1	8.595
5	C_3H_6S	74.0190	1	0.693
6	C_3H_8S	76.0346	1	1.188
7	CH_2S_2	77.9597	2	0.081
8	CH_4S_2	79.9754	2	0.044
9	$C_2H_4S_2$	91.9754	2	0.186
10	$C_2H_6S_2$	93.9910	2	0.324
11	$C_3H_4S_2$	103.9754	2	0.248
12	$C_3H_6S_2$	105.9910	2	0.688
13	$C_3H_8S_2$	108.0067	2	0.305
14	$C_5H_8S_2$	132.0067	2	0.063
15	$C_6H_{14}S_2$	150.0536	2	0.783
16	$C_2H_6S_3$	125.9631	3	0.067
17	$C_3H_6S_3$	137.9631	3	0.062
18	$C_4H_{10}S_3$	153.9944	3	0.495
19	$C_2H_6S_4$	157.9352	4	0.008
20	$C_3H_6S_4$	169.9352	4	0.006

240

Table S5. Oxidation products formed from the •OH-initiated oxidation of freshwater algae-emitted VOCs and detected by nitrate-CI-LToF-MS.

Species	Molecular formula	Molecular mass	Mass Defect	Normalized value
Multi-sulfur products	$C_3H_8O_2S_2$	139.9965	-0.00343	1.66E-03
	$C_2H_6O_3S_2$	141.9758	-0.02416	1.36E-04
	$C_4H_{10}O_2S_2$	154.0122	0.01222	1.71E-05
	$C_2H_4O_4S_2$	155.9551	-0.04490	9.15E-06
	$C_3H_8O_3S_2$	155.9914	-0.00851	3.82E-05
	$C_3H_8O_2S_3$	171.9686	-0.03136	1.23E-04
	$C_6H_{12}O_2S_2$	180.0278	0.02787	4.58E-05
	$C_6H_{14}O_2S_2$	182.0435	0.04352	1.68E-05
	$C_3H_8O_3S_3$	187.9635	-0.03644	1.09E-05
	$C_2H_6O_7S_2$	205.9554	-0.04451	7.61E-06
	$C_{10}H_{22}O_3S_3$	286.0731	0.07311	3.57E-05
Mono-sulfur products	CH_4O_3S	95.9881	-0.01188	2.42E-02
	$C_2H_4O_3S$	107.9881	-0.01188	6.54E-05
	CH_2O_4S	109.9673	-0.03262	1.69E-05
	CH_4O_4S	111.9830	-0.01697	2.12E-04
	$C_3H_6O_3S$	122.0037	0.00377	6.85E-05
	$C_3H_8O_3S$	124.0194	0.01941	4.01E-04
	$C_3H_6O_4S$	137.9986	-0.00132	6.21E-06
	$C_2H_4O_5S$	139.9779	-0.02206	1.13E-05
	$C_3H_8O_4S$	140.0143	0.01433	5.95E-05
	$C_3H_4O_5S$	151.9779	-0.02206	1.10E-05
	$C_3H_6O_5S$	153.9935	-0.00641	2.00E-05
	$C_2H_4O_6S$	155.9728	-0.02714	1.70E-05
	$C_3H_8O_5S$	156.0092	0.00924	9.78E-06
	$C_4H_6O_6S$	181.9885	-0.01149	4.22E-06
	$C_7H_{12}O_5S$	208.0405	0.04054	6.29E-06
	$C_6H_{12}O_7S$	228.0303	0.03037	4.18E-06
	$C_9H_{12}O_5S$	232.0405	0.04054	1.93E-04
	$C_{12}H_{12}O_3S$	236.0507	0.05071	1.19E-04
	$C_7H_{10}O_7S$	238.0147	0.01472	8.62E-06
	$C_{12}H_{14}O_3S$	238.0663	0.06636	2.22E-04
	$C_{13}H_{14}O_3S$	250.0663	0.06636	2.68E-04
	$C_{12}H_{14}O_4S$	254.0612	0.06128	1.52E-04
	$C_{13}H_{18}O_3S$	254.0976	0.09766	2.81E-04
	$C_{13}H_{14}O_4S$	266.0612	0.06128	7.47E-05
	$C_{13}H_{16}O_4S$	268.0769	0.07693	7.64E-04
	$C_9H_{18}O_7S$	270.0773	0.07732	1.61E-05

Inorganic sulfur products and clusters	H_2SO_3	81.9724	-0.02754	3.53E-05
	H_2SO_4	97.9673	-0.03262	4.40E-03
	H_2SO_5	113.9622	-0.03771	1.78E-04
	$(CH_4O_3S)_2$	191.9762	-0.02377	1.82E-04
	$H_2SO_4 \cdot CH_4O_3S$	193.9554	-0.04451	1.50E-03
	$(H_2SO_4)_2$	195.9347	-0.06524	2.24E-04
Other products	$C_2H_4O_3$	76.0160	0.01604	8.44E-06
	$C_2H_2O_4$	89.9953	-0.00469	5.14E-06
	$C_3H_6O_3$	90.0316	0.03169	2.18E-06
	$C_2H_4O_4$	92.0109	0.01096	1.18E-06
	$C_2H_6O_4$	94.0266	0.02661	3.93E-06
	$C_4H_4O_3$	100.0160	0.01604	4.62E-06
	$C_3H_2O_4$	101.9953	-0.00469	2.71E-05
	$C_4H_6O_3$	102.0316	0.03169	5.87E-06
	$C_3H_5NO_3$	103.0269	0.02694	8.31E-06
	$C_3H_4O_4$	104.0109	0.01096	1.03E-04
	$C_4H_8O_3$	104.0473	0.04734	1.07E-06
	$C_5H_4O_3$	112.0160	0.01604	1.50E-06
	$C_4H_4O_4$	116.0109	0.01096	5.14E-06
	$C_3H_4N_2O_3$	116.0221	0.02219	1.10E-04
	$C_5H_8O_3$	116.0473	0.04734	4.85E-06
	$C_4H_7NO_3$	117.0425	0.04259	1.61E-06
	$C_2H_2N_2O_4$	118.0014	0.00146	2.72E-06
	$C_4H_6O_4$	118.0266	0.02661	3.39E-06
	$C_3H_4O_5$	120.0058	0.00587	1.94E-05
	$C_3H_6O_5$	122.0215	0.02152	1.04E-05
	$C_3H_8O_5$	124.0371	0.03717	7.38E-04
	$C_5H_7NO_3$	129.0425	0.04259	4.59E-06
	$C_5H_6O_4$	130.0266	0.02661	3.42E-05
	$C_6H_{10}O_3$	130.0629	0.06299	2.14E-06
	$C_5H_9NO_3$	131.0582	0.05824	3.55E-06
	$C_4H_4O_5$	132.0058	0.00587	3.08E-06
	$C_5H_8O_4$	132.0422	0.04226	8.71E-06
	$C_4H_6O_5$	134.0215	0.02152	2.16E-06
	$C_4H_8O_5$	136.0371	0.03717	4.89E-05
	$C_7H_6O_3$	138.0316	0.03169	9.26E-05
	$C_6H_6O_4$	142.0266	0.02661	2.17E-05
	$C_7H_{10}O_3$	142.0629	0.06299	1.39E-05
	$C_6H_8O_4$	144.0422	0.04226	7.22E-06
	$C_5H_6O_5$	146.0215	0.02152	2.67E-06
	$C_5H_8O_5$	148.0371	0.03717	2.18E-05
	$C_7H_6O_4$	154.0266	0.02661	1.03E-05

	$C_6H_4O_5$	156.0058	0.00587	6.71E-06
	$C_7H_8O_4$	156.0422	0.04226	5.65E-06
	$C_6H_6O_5$	158.0215	0.02152	1.43E-05
	$C_7H_{10}O_4$	158.0579	0.05791	9.18E-06
	$C_6H_8O_5$	160.0371	0.03717	1.03E-05
	$C_5H_6O_6$	162.0164	0.01644	1.27E-05
	$C_7H_{14}O_4$	162.0892	0.08921	2.90E-06
	$C_6H_{12}O_5$	164.0684	0.06847	2.20E-05
	$C_8H_8O_4$	168.0422	0.04226	3.15E-06
	$C_7H_6O_5$	170.0215	0.02152	1.93E-05
	$C_8H_{10}O_4$	170.0579	0.05791	1.11E-05
	$C_7H_8O_5$	172.0371	0.03717	1.56E-06
	$C_8H_{12}O_4$	172.0735	0.07356	2.04E-05
	$C_8H_{14}O_4$	174.0892	0.08921	6.53E-05
	$C_8H_6O_5$	182.0215	0.02152	1.06E-05
	$C_6H_6O_7$	190.0113	0.01135	1.75E-05
	$C_8H_{14}O_5$	190.0841	0.08412	3.53E-05
	$C_6H_{10}O_7$	194.0426	0.04265	8.42E-05
	$C_{10}H_{14}O_4$	198.0892	0.08921	7.19E-06
	$C_8H_8O_6$	200.0320	0.03209	3.35E-05
	$C_8H_{10}O_6$	202.0477	0.04774	1.71E-04
	$C_8H_{12}O_6$	204.0633	0.06339	2.93E-04
	$C_9H_{16}O_5$	204.0997	0.09977	3.93E-05
	$C_7H_{10}O_7$	206.0426	0.04265	4.72E-05
	$C_{11}H_{10}O_4$	206.0579	0.05791	1.88E-06
	$C_8H_{14}O_6$	206.0790	0.07904	8.90E-05
	$C_9H_{18}O_5$	206.1154	0.11542	5.79E-05
	$C_7H_{12}O_8$	224.0532	0.05322	4.13E-05
	$C_{12}H_{10}O_7$	266.0426	0.04265	3.78E-05
	$C_{10}H_{10}O_9$	274.0324	0.03248	7.89E-06
	$C_{12}H_{20}O_7$	276.1209	0.12090	4.29E-06

243

References

Atkinson, R., Baulch, D. L., Cox, R. A., Crowley, J. N., Hampson, R. F., Hynes, R. G., Jenkin, M. E., Rossi, M. J., and Troe, J.: Evaluated kinetic and photochemical data for atmospheric chemistry: Volume I - gas phase reactions of O_x, HO_x, NO_x and SO_x species, Atmos. Chem. Phys., 4, 1461–1738, https://doi.org/10.5194/acp-4-1461-2004, 2004.

Crounse, J. D., Nielsen, L. B., Jørgensen, S., Kjaergaard, H. G., and Wennberg, P. O.: Autoxidation of Organic Compounds in the Atmosphere, J. Phys. Chem. Lett., 4, 3513–3520, https://doi.org/10.1021/jz4019207, 2013.

Jacob, L. S. D., Giorio, C., and Archibald, A. T.: Extension, development, and evaluation of the representation of the OH-initiated dimethyl sulfide (DMS) oxidation mechanism in the Master Chemical Mechanism (MCM) v3.3.1 framework, Atmos. Chem. Phys., 24, 3329–3347, https://doi.org/10.5194/acp-24-3329-2024, 2023.

Jenkin, M. E., Young, J. C., and Rickard, A. R.: The MCM v3.3.1 degradation scheme for isoprene, Atmos. Chem. Phys., 15, 11433–11459, https://doi.org/10.5194/acp-15-11433-2015, 2015.

Lambe, A. T., Ahern, A. T., Williams, L. R., Slowik, J. G., Wong, J. P. S., Abbatt, J. P. D., Brune, W. H., Ng, N. L., Wright, J. P., Croasdale, D. R., Worsnop, D. R., Davidovits, P., and Onasch, T. B.: Characterization of aerosol photooxidation flow reactors: heterogeneous oxidation, secondary organic aerosol formation and cloud condensation nuclei activity measurements, Atmos. Meas. Tech., 4, 445–461, https://doi.org/10.5194/amt-4-445-2011, 2011.

Lightfoot, P. D., Cox, R. A., Crowley, J. N., Destriau, M., Hayman, G. D., Jenkin, M. E., Moortgat, G. K., and Zabel, F.: Organic peroxy radicals: Kinetics, spectroscopy and tropospheric chemistry, Atmos. Environ. Part A Gen. Top., 26, 1805–1961, https://doi.org/10.1016/0960-1686(92)90423-i, 1992.

Orlando, J. J. and Tyndall, G. S.: Laboratory studies of organic peroxy radical chemistry: an overview with emphasis on recent issues of atmospheric significance, Chem. Soc. Rev., 41, 6294, https://doi.org/10.1039/c2cs35166h, 2012.

Saunders, S. M., Jenkin, M. E., Derwent, R. G., and Pilling, M. J.: Protocol for the development of the Master Chemical Mechanism, MCM v3 (Part A): tropospheric degradation of non-aromatic volatile organic compounds, Atmos. Chem. Phys., 3, 161–180, https://doi.org/10.5194/acp-3-161-2003, 2003.